

Review

# Suppressing lithium dendrites within inorganic solid-state electrolytes

Qiang Lv,<sup>1</sup> Yunpeng Jiang,<sup>1</sup> Bo Wang,<sup>1,7,\*</sup> Yujia Chen,<sup>1</sup> Fan Jin,<sup>1</sup> Bochen Wu,<sup>1</sup> Huaizheng Ren,<sup>1</sup> Nan Zhang,<sup>1</sup> Ruoyu Xu,<sup>2</sup> Yaohua Li,<sup>3</sup> Tianren Zhang,<sup>4</sup> Yu Zhou,<sup>5</sup> Dianlong Wang,<sup>1,\*</sup> Huakun Liu,<sup>6</sup> and Shixue Dou<sup>6</sup>

## SUMMARY

The Li metal anode possesses the high specific capacity and the minimum reduction potential known as the renaissance of high-energy-density battery. However, the security problems brought by uncontrolled Li dendrites have hindered its development. Integrating the Li metal anode with non-flammable solid-state electrolytes (SSEs) provides a promising approach to solve the problem of Li dendrites and achieve safe Li metal batteries. However, recent studies indicate that Li dendrites still occur in the interior of inorganic SSEs, although the high mechanical strength of inorganic SSEs can resist dendrite growth in theory. In this review, the main causes of Li dendrites within inorganic SSEs are summarized. Combined with advanced characterization techniques and theoretical calculations, theoretical models of Li dendrite growth within SSEs are clarified. Furthermore, various strategies for suppressing Li dendrites are comprehensively summarized. Finally, the research prospects of dendrite-free all-solid-state Li metal batteries are evaluated.

## INTRODUCTION

A rechargeable liquid Li battery ( $\text{Li}||\text{TiS}_2$ ) was constructed by Whittingham for the first time in 1976, which showed a high energy density of nearly  $500 \text{ Wh kg}^{-1}$ .<sup>1</sup> After several years of iteration, Li metal batteries were introduced into the electric vehicle industry by Moli Energy.<sup>2,3</sup> However, these Li metal batteries were recalled due to safety issues.<sup>4,5</sup> Soon after, Li-ion battery was invented in 1985, which consisted of a  $\text{LiCoO}_2$  cathode developed by Goodenough and a carbonaceous anode developed by Yoshino.<sup>6,7</sup> The “rocking chair”-type charge and discharge of the Li-ion battery exhibited better stability than that of Li metal battery. Taking advantage of the long-term cyclic stability of the Li-ion battery, Sony, with its 18650 battery, quickly occupied the commercial market.<sup>8</sup> Since then, Li-ion batteries based on carbonaceous anodes have been constantly iterated to now. Nevertheless, with rapid development of the cathodes (such as  $\text{LiFePO}_4$ ,<sup>9</sup>  $\text{LiNi}_{1-x-y}\text{Co}_x\text{Mn}_y\text{O}_2$ ,<sup>10</sup> etc.), Li-ion batteries with carbonaceous-based anodes gradually approached the upper limit of energy density ( $\sim 250 \text{ Wh kg}^{-1}$ ).<sup>11</sup>

Recently, the introduction of Si-based anodes has been found to increase the energy density of a battery to more than  $300 \text{ Wh kg}^{-1}$ , marking a major milestone in the development of Li-ion batteries.<sup>12</sup> However, once Li metal as the anode (with the high theoretical capacity of nearly  $3860 \text{ mAh g}^{-1}$  or  $2061 \text{ mAh cm}^{-3}$  and the lowest electrochemical potential of nearly  $-3.04 \text{ V}$  versus the standard hydrogen electrode)<sup>13,14</sup> paired with the recently developed S-based or  $\text{O}_2$  cathodes, energy

<sup>1</sup>MIIT Key Laboratory of Critical Materials Technology for New Energy Conversion and Storage, State Key Laboratory of Urban Water Resource and Environment, School of Chemistry and Chemical Engineering, Harbin Institute of Technology, Harbin 150001, China

<sup>2</sup>Department of Chemical Engineering, University College London, Torrington Place, London WC1E 6BT, United Kingdom

<sup>3</sup>Department of Materials Science and Engineering, Northwestern University, Evanston, IL 60208, United States

<sup>4</sup>Tianneng Group, Huzhou 313000, China

<sup>5</sup>School of Materials Science and Engineering, Harbin Institute of Technology, Harbin 150001, China

<sup>6</sup>Institute for Superconducting & Electronic Materials, Australian Institute of Innovative Materials, University of Wollongong, Wollongong, NSW 2500, Australia

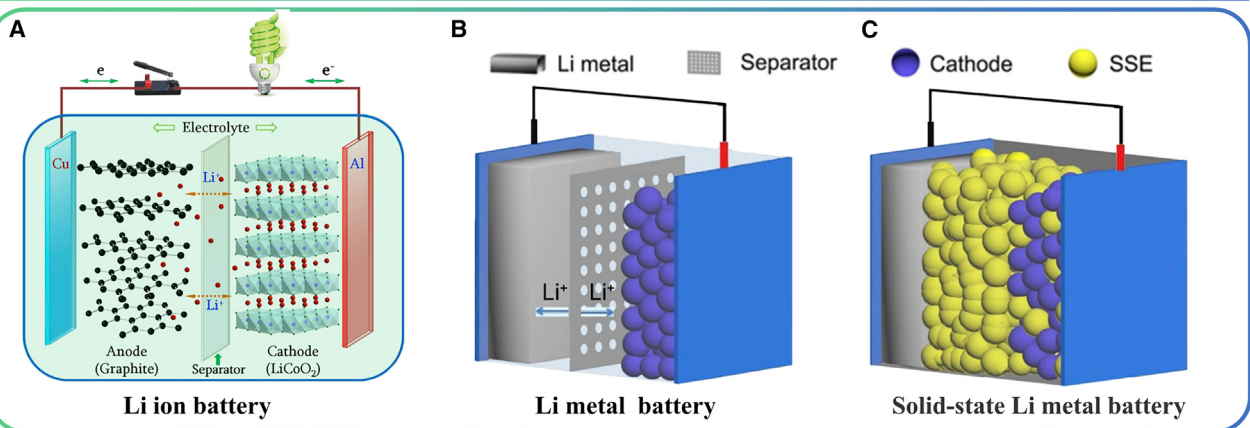
<sup>7</sup>Lead contact

\*Correspondence:  
[wangbo19880804@163.com](mailto:wangbo19880804@163.com) (B.W.),  
[wangdianlonghit@163.com](mailto:wangdianlonghit@163.com) (D.W.)

<https://doi.org/10.1016/j.xcpr.2021.100706>



## Working mechanisms of different Li battery systems



## Evaluation of different Li battery systems

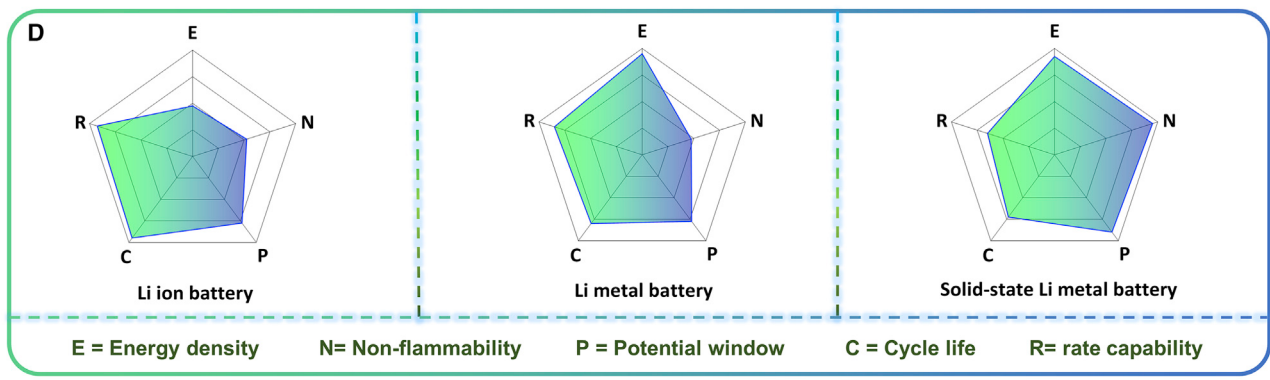


**Figure 1. Working mechanisms and evaluation of different Li battery systems**

(A) Working mechanism of Li ion battery. Reproduced with permission from Liu et al.<sup>33</sup> Copyright 2016, Elsevier.

(B) Working mechanism of Li metal battery.

(C) Working mechanism of solid-state Li metal battery. Reproduced with permission from Miao et al.<sup>34</sup> Copyright 2020, The Royal Society of Chemistry.  
(D) Evaluation of different Li battery systems.

densities of  $\sim 650 \text{ Wh kg}^{-1}$  and  $\sim 950 \text{ Wh kg}^{-1}$  can be achieved (Figure 1).<sup>11</sup> Unfortunately, the security problems brought by uncontrolled Li dendrite growth have seriously hindered the application of the Li metal anode.<sup>15</sup> Various strategies (such as artificial solid-electrolyte interfaces<sup>16–19</sup>, structured lithophilic hosts<sup>20–22</sup>, liquid electrolyte engineering<sup>23–28</sup>, and solid-state electrolytes<sup>29,30</sup>) have been developed to solve the problem of Li dendrites.<sup>31,32</sup>

Among the above-mentioned strategies, although it still falls short in high-rate performance compared with flammable liquid electrolytes, non-flammable solid-state electrolytes (SSEs) are widely expected to solve the security problems brought by insufficient thermal stability and the growth of Li dendrites.<sup>35–40</sup> Furthermore, SSEs also show better electrochemical stability.<sup>38,39</sup> Solid polymer electrolytes (SPEs), with superior flexibility and favorable membrane-forming capability, have been extensively studied.<sup>41,42</sup> However, the low ionic conductivity of SPEs and the issue of dendrite-penetration through soft SPEs with low shear modulus limit the practical application of SPEs.<sup>43–46</sup> Inorganic SSEs with high ionic conductivity ( $\text{Li}_{10}\text{GeP}_2\text{S}_{12}$   $\sim 12 \text{ mS cm}^{-1}$ ,<sup>47</sup>  $\text{Li}_7\text{P}_3\text{S}_{11}$   $\sim 17 \text{ mS cm}^{-1}$ <sup>48</sup>) and high shear modulus ( $\text{Li}_3\text{PS}_4$   $\sim 12 \text{ GPa}$ ,<sup>49</sup>

$\text{Li}_7\text{La}_3\text{Zr}_2\text{O}_{12}$ ~100 GPa<sup>50</sup>) hold great hope to resist dendrite growth and achieve the practical application of all-solid-state Li metal batteries.<sup>51–55</sup> Nevertheless, with the advancement of characterization techniques, Li dendrites are still found in the bulk phase of inorganic SSEs, which gradually grow and penetrate through SSEs, finally leading to short-circuit and cell failures. Therefore, researchers have conducted in-depth research on the Li dendrites in the interior of inorganic SSEs.<sup>56,57</sup> It is found that the growth of Li dendrites within inorganic SSEs is related to the voids and pores, grain boundaries, cracks, electronic conductivity, and critical current density.<sup>58</sup>

Moreover, several reviews have rarely involved Li dendrites in the interior of inorganic SSEs.<sup>46,59,60</sup> Among them, there are two targeted reviews on Li dendrites within SSEs, which only summarize from the perspective of inorganic and organic SSEs.<sup>61–63</sup> However, systematic analysis for the causes of Li dendrites growth within inorganic SSEs is still relatively scarce. And endless theoretical models and advanced characterizations in recent years have emerged to accurately interpret the Li dendrites in the bulk phase of inorganic SSEs. Therefore, this review focuses on summarizing the main causes of Li dendrite growth within inorganic SSEs. Combined with theoretical calculations and advanced characterizations, mechanistic models of Li dendrite growth within SSEs are further clarified. Finally, the corresponding strategies of suppressing Li dendrites are comprehensively summarized, and the research prospects of dendrite-free all-solid-state Li metal batteries are evaluated (Figure 2).

## CAUSES OF LI DENDRITES WITHIN INORGANIC SSEs

Compared to soft polymer electrolytes, inorganic SSEs can better resist Li dendrites due to its high shear modulus in theory.<sup>70</sup> However, researchers discovered a voltage drop during polarization in garnet-based ( $\text{Li}_7\text{La}_3\text{Zr}_2\text{O}_{12}$ –LLZO) all-solid-state batteries as the current density increased, which was attributed to short-circuiting of the battery caused by Li dendrites within SSEs.<sup>71</sup> Combined with the theoretical simulations and advanced characterizations, the growth of Li dendrites have also been gradually observed in the bulk phase of other inorganic SSEs.<sup>67,72,73</sup> Therefore, it is necessary to systematically analyze the causes of the Li dendrite growth within inorganic SSEs.<sup>74</sup> According to previously reported studies, the causes of the growth of Li dendrites within inorganic SSEs can be summarized into the following categories.

### Macroscopic defects

It is well known that the high shear modulus of completely compact inorganic SSEs can resist the growth of Li dendrites in theory. However, there are always various defects for practical SSEs. Researchers discovered that macroscopic defects including the voids and pores promoted the growth of Li dendrites within SSEs.<sup>75</sup> Ren et al.<sup>56</sup> found that once there are voids and pores, the Li dendrites will penetrate through the interconnected pores and voids within ceramic electrolyte ( $\text{Li}_{6.75}\text{La}_3\text{Zr}_{1.75}\text{Ta}_{0.25}\text{O}_{12}$ –LLZTO) and grow along the porous grain boundary (Figures 3A and 3B).

Furthermore, recent research has shown that the growth of Li dendrites would fill all the voids and pores, and then penetrated from the interior of the SSEs to the cathode, resulting in short-circuit of the battery. Intriguingly, the period before short-circuit of the battery occurs is positively correlated with the relative density of SSEs, which is estimated based on the ratio of the density calculated from the lattice constant to the density calculated from the weight and volume. Moreover, the  $\text{Al}_2\text{O}_3$ -doped  $\text{Li}_7\text{La}_3\text{Zr}_2\text{O}_{12}$  has shown that a long period before short-circuit of the battery occurs is due to the improved relative density.<sup>71</sup>

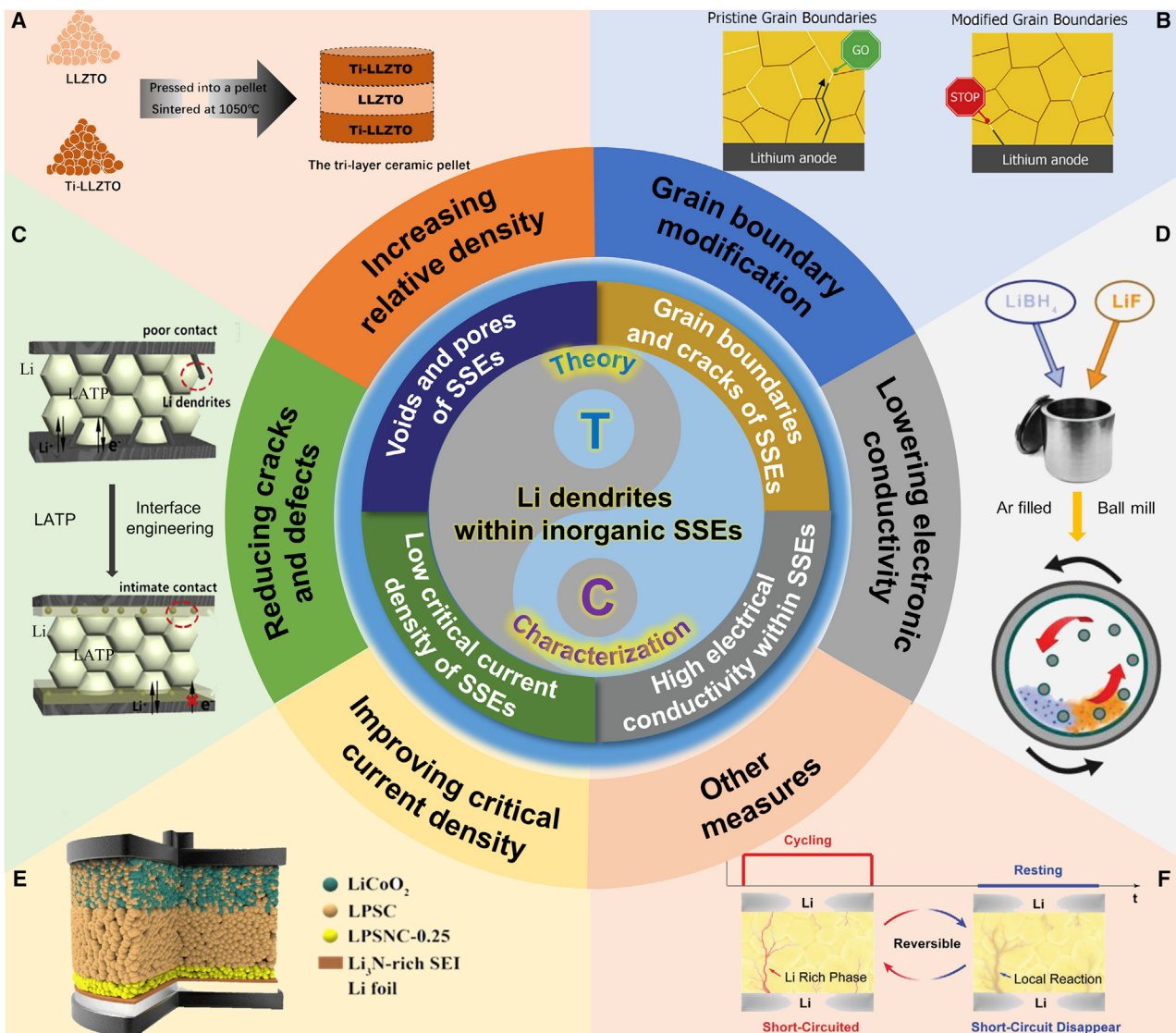


**Figure 2. Schematic illustration of the outline for suppressing Li dendrites within inorganic SSEs**

(A) Multilayer ceramic electrolyte increases relative density of SSEs. Reproduced with permission from Zhu et al.<sup>64</sup> Copyright 2020, Wiley-VCH.

(B) Grain boundary modification. Reproduced with permission from Hongahally et al.<sup>65</sup> Copyright 2017, Elsevier.

(C) Interface engineering inhibits Li penetration. Reproduced with permission from Jin et al.<sup>66</sup> Copyright 2021, The Royal Society of Chemistry.

(D) Adding LiF lowers electronic conductivity of SSEs. Reproduced with permission from Mo et al.<sup>67</sup> Copyright 2019, Wiley-VCH.

(E) *In situ* interface rich in Li<sub>3</sub>N increases critical current density. Reproduced with permission from Liu et al.<sup>68</sup> Copyright 2021, The Royal Society of Chemistry.

(F) Reversible short-circuit in garnet solid-state batteries. Reproduced with permission from Ping et al.<sup>69</sup> Copyright 2020, Wiley-VCH.

Therefore, there is reason to believe that high shear modulus is not enough to completely inhibit Li dendrite growth in the interior of inorganic SSEs. And macroscopic defects including voids and pores should be appropriately suppressed.

### Micro defects

Nevertheless, the SSEs with high relative density cannot completely inhibit Li dendrite penetration through SSEs caused by micro defects such as grain boundaries (GBs) and cracks.<sup>82,83</sup> Researchers discovered that Li dendrites nucleated and formed at GBs and cracks, and gradually penetrated through inorganic SSEs, resulting in short-circuit of the battery.<sup>84</sup>

### Causes of Li dendrites within inorganic SSEs

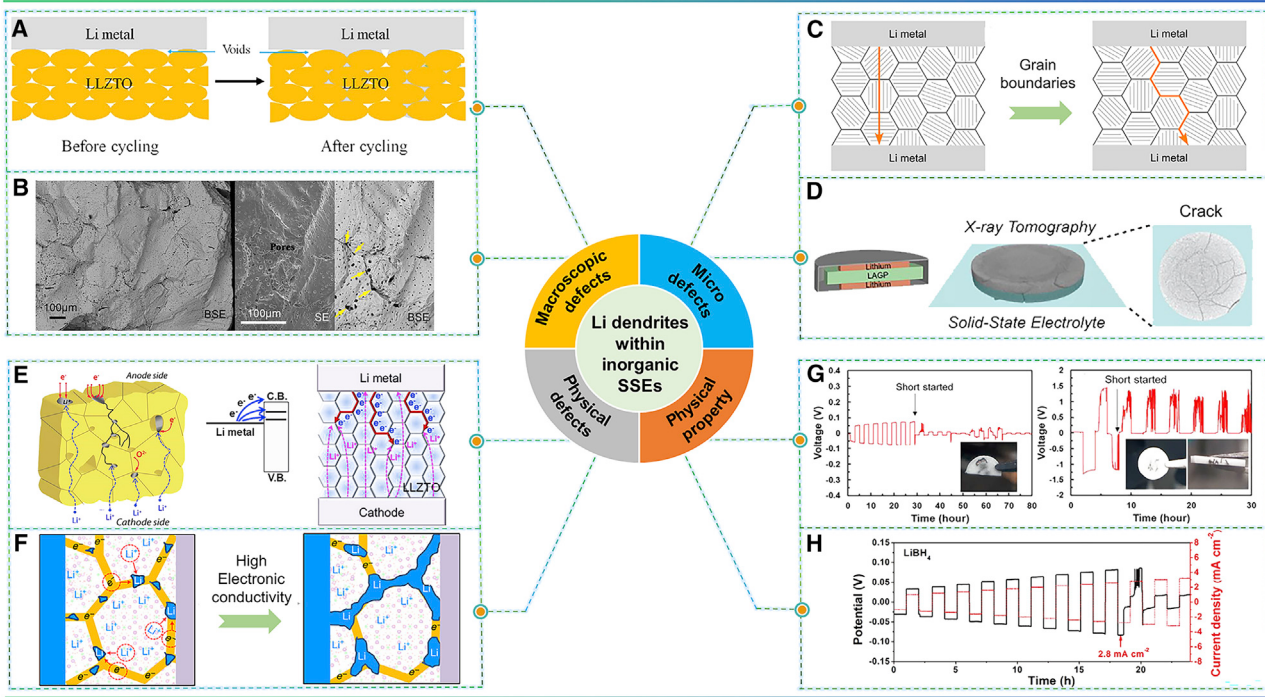


**Figure 3. The causes of Li dendrites growth within inorganic SSEs**

(A) Schematics showing Li deposition of  $\text{Li}_{6.75}\text{La}_3\text{Zr}_{1.75}\text{Ta}_{0.25}\text{O}_{12}$ (LLZTO) particles solid state electrolyte. Reproduced with permission from Tian et al.<sup>76</sup> Copyright 2018, Elsevier.

(B) Cross-sectional SEM micrographs of the short-circuit in garnet solid-state batteries. Reproduced with permission from Ren et al.<sup>56</sup> Copyright 2015, Elsevier.

(C) Illustration of Li metal plating based on polycrystalline LLZO solid-state electrolyte. Reproduced with permission from Cheng et al.<sup>77</sup> Copyright 2017, Elsevier.

(D) *In situ* X-ray micro imaging of Li/LAGP/Li symmetric batteries. Reproduced with permission from Tippens et al.<sup>78</sup> Copyright 2019, American Chemical Society.

(E) Schematic of the cross section in garnet ceramic electrolyte (left). Reproduced with permission from Aguesse et al.<sup>73</sup> Copyright 2017, American Chemical Society. Schematic illustration of Li propagation along GBs of LLZTO (right). Reproduced with permission from Kim et al.<sup>79</sup> Copyright 2020, The Royal Society of Chemistry.

(F) Mechanism of Li filament formation and Li penetration within polycrystalline electrolytes. Reproduced with permission from Liu et al.<sup>80</sup> Copyright 2021, Nature Publishing Group.

(G) Cyclic performance of Li/LLZO/Li and Li/LATP/Li symmetric batteries. Reproduced with permission from Wu et al.<sup>81</sup> Copyright 2018, The Royal Society of Chemistry.

(H) Electrochemical cycling curves of  $\text{LiBH}_4$  at step-increased current densities. Reproduced with permission from Mo et al.<sup>67</sup> Copyright 2020, Wiley-VCH.

Li dendrites easily nucleate at the defects of GBs and subsequently penetrate the entire SSE along the pre-existing defects of GBs, whether it is single crystal or polycrystalline, causing a short-circuit of the battery.<sup>85–87</sup> Furthermore, the penetrative mode of Li dendrites within polycrystalline SSEs is influenced by the mechanical properties and microstructure of the GBs (Figure 3C).<sup>72</sup> Due to the softening of the GBs, the compressive stress at the interface and the shear modulus at GBs is reduced. Consequently, Li metal nucleates at GB and Li/SSEs interface and gradually penetrates through SSEs.<sup>82</sup> In addition, excessive trapping of electrons at GBs would trigger the nucleation of Li dendrites and increase the penetrating depth of Li dendrites.<sup>75,77</sup>

Cracks are another reason to promote Li dendrites penetration in the interior of inorganic SSEs. Based on the mechanical crack mechanism, once the cracks occur within

inorganic SSEs, the Li filaments would grow along cracks and gradually penetrate SSEs and ultimately leads to short-circuit of the battery (Figure 3D).<sup>88</sup>

To conclude, micro defects like GB and cracks contribute to Li dendrite growth and penetration in the bulk phase of inorganic SSEs; therefore, they require inhibition as well.

### Physical defects

Ideal SSEs with high mechanical strength and low electrical conductivity could inhibit the growth of Li dendrites. However, physical defects such as high local electronic conductivity of SSEs could directly reduce  $\text{Li}^+$  to Li metal in the bulk phase of inorganic SSEs and gradually form Li dendrites within inorganic SSEs.<sup>63</sup>

John A. Kilner et al.<sup>73</sup> put forward that partial electronic conductivity of crystalline SSEs could provide electronic conductive pathways for Li nucleation within inorganic SSEs (Figure 3E). In other words, where there are electrons, there will be continuous Li nucleation and deposition. In addition, Wang's group also proved that the high electronic conductivity of  $\text{Li}_3\text{PS}_4$  and  $\text{Li}_7\text{La}_3\text{Zr}_2\text{O}_{12}$  was mostly responsible for dendrite formation in these SSEs.<sup>89</sup> Generally, it was assumed that the high electronic conductivity of SSEs provided an electronic pathway for the direct reduction of  $\text{Li}^+$  to Li metal at grain boundary/pore of SSEs, and Li dendrites gradually formed and permeated through entire SSEs, eventually leading to short-circuit of the battery (Figure 3F).<sup>67,90</sup>

Therefore, it is necessary to lower the electrical conductivity of SSEs to suppress Li dendrites in the bulk phase of inorganic SSEs.

### Physical property

The formation of Li dendrites is also related to physical property, such as critical current density (CCD). The maximum endurable current density of Li metal batteries cycling without cell failures in all-solid-state Li batteries is generally defined as CCD (usually reported as less than  $1\text{ mA cm}^{-2}$ ).<sup>59,91–93</sup> Once the applied current density is larger than CCD, SSEs will not transport enough  $\text{Li}^+$  in time for reaction, resulting in large concentration polarization and electron accumulation, and then leading to Li dendrite nucleation and penetration and short-circuit of the battery (Figures 3G and 3H).<sup>67</sup>

All-solid-state Li batteries with inorganic SSEs show high cyclic stability and high coulomb efficiency at low current densities. However, Li dendrite growth still occurred in the bulk phase of inorganic SSEs at high current densities, even though the high mechanical strength of inorganic SSEs could resist dendrite growth in theory. Due to the smaller CCD than organic electrolytes, Li dendrites are more likely to form within inorganic SSEs, especially at high current densities. For example, the CCD values of  $\text{Li}_7\text{La}_3\text{Zr}_2\text{O}_{12}$  ( $0.05$  to  $0.9\text{ mA cm}^{-2}$ ) and  $\text{Li}_2\text{S-P}_2\text{S}_5$  ( $0.4$  to  $1\text{ mA cm}^{-2}$ ) are much lower than that of organic electrolytes ( $3$  to  $10\text{ mA cm}^{-2}$ ).<sup>94</sup>

Therefore, other strategies are required to improve the CCD of SSEs and inhibit Li dendrite growth within inorganic SSEs.

## ADVANCED CHARACTERIZATION TECHNIQUES AND THEORETICAL MODELS

Different from batteries with liquid electrolytes, initial growth of Li dendrites can either happen in the interface of Li/SSEs interface or in the interior of SSEs. With the help of advanced characterization techniques and theoretical simulations, the

theoretical models and the main causes of Li dendrites within SSEs have been gradually analyzed and clarified.

### Advanced characterization techniques

Advanced characterization techniques play an important role in the analysis of Li dendrites growth within SSEs. The main directions of characterization are: (1) observing and confirming Li dendrite growth within SSEs and (2) elucidating the causes of Li dendrites within SSEs.

With the continuous efforts of researchers and the gradual application of advanced characterizations, Li dendrites within SSEs have been observed in short-circuited batteries.<sup>95</sup> For the first time, Li dendrites in the interior of polymer electrolytes were observed in short-circuited batteries by using *in situ* scanning electron microscopy (SEM) in 2002 (Figure 4A). It was shown that Li dendrite growth at the interface could further penetrate through soft polymer electrolytes with insufficient shear modulus. Similarly, Nagao et al.<sup>72</sup> directly observed columnar Li deposition in short-circuited battery based on Li<sub>2</sub>S–P<sub>2</sub>S<sub>5</sub> by using SEM in 2013 (Figure 4B). Furthermore, optical microscopy and *in situ* mini cell were also used to observe the Li dendrites growth within optically SSEs.<sup>96,97</sup> After that, dual-beam (Focused ion beam) FIB-SEM revealed that the hard and hollow Li dendrites could penetrate through soft polymer electrolytes in the short-circuited battery (Figure 4D).<sup>98</sup> Besides, atomic force microscopy (AFM) combined with environmental transmission electron microscopy (TEM) was used to observe the *in situ* growth of individual Li whiskers in the bulk phase of SSEs, which provides a quantitative benchmark for inhibiting Li dendrite growth within SSEs.<sup>74</sup>

Although Li dendrites within SSEs have been observed in short-circuited batteries, it is necessary to provide the direct evidence by advanced characterizations to prove that the growth of dendrites within SSEs is Li metal. High resolution transmission electron microscope (TEM) and electron energy loss spectroscopy (EELS) was first be used to confirm that Li dendrites growth at GBs of Li<sub>6.75</sub>La<sub>3</sub>Zr<sub>1.75</sub>Ta<sub>0.25</sub>O<sub>12</sub>(LLZTO) in 2016 (Figure 4C).<sup>75</sup> Then, Auger electron spectroscopy (AES) with precise chemical sensitivity<sup>77</sup> and non-destructive neutron depth profiling (NDP) analysis technology were used to prove that Li propagates preferably along the grain boundary of Li<sub>7</sub>-La<sub>3</sub>Zr<sub>2</sub>O<sub>12</sub>(LLZO) during cycling, resulting in the short-circuit of Li/LLZO/Li symmetric battery (Figures 4E and 4F).<sup>99</sup> Besides, Marbella et al.<sup>100</sup> confirmed that short-circuit of the battery was obviously related to Li dendrites within LLZTO by using <sup>7</sup>Li Nuclear magnetic resonance (NMR) chemical shift imaging in 2019 (Figure 4G).<sup>103</sup>

Visualizing the process of reaction within SSEs is also helpful to understand the growth of Li dendrites within SSEs. *In situ* X-ray computed tomography in micro nanoscale<sup>78</sup> and *in situ* space X-ray diffraction<sup>101</sup> were first used to visualize the process of crack evolution in the interior of SSEs, which included Li deposition and Li dendrites penetration (Figures 4H and 4I). Besides, *in situ* microscopic and cryo-TEM were reported to provide visual evidence for the dynamic process of Li dendrites formation and penetration within SSEs in 2021 (Figure 4J).<sup>102</sup>

After the discoveries and confirmations of Li dendrites within SSEs, advanced characterization techniques have also been used to reveal the causes of this phenomenon. Among them, X-ray tomography was first widely used. Synchrotron X-ray micro tomography technology was first used in 2014 to prove that the unstable interface of Li/polymer electrolytes induced Li dendrite growth at the interface and further penetrated through soft polymer electrolytes with insufficient shear modulus in Figure 5A.<sup>104</sup> Similarly, synchrotron X-ray tomography was used in 2018 to confirm

**Characterizations for directly observing and confirming Li dendrites within SSEs**

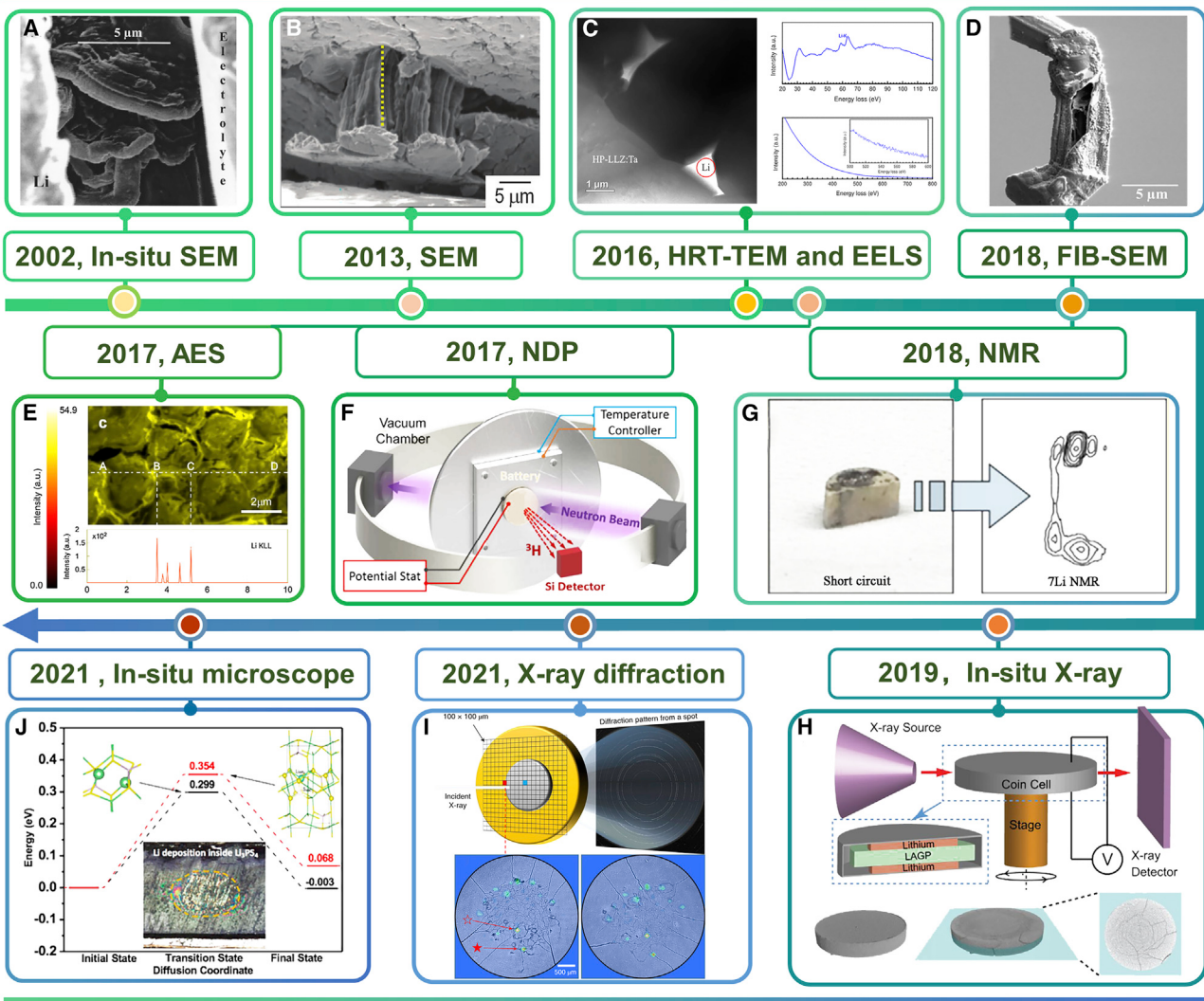


**Figure 4. Advanced characterization techniques for observing and confirming Li dendrite growth within SSEs**

- (A) *In situ* SEM observing Li dendrite growth through polymer SSEs. Reproduced with permission from Mickal et al.<sup>95</sup> Copyright 2002, Electrochemical Society Active Member
- (B) SEM showing the columnar Li deposition in  $\text{Li}_2\text{S}-\text{P}_2\text{S}_5$ . Reproduced with permission from Nagao et al.<sup>72</sup> Copyright 2013, The Royal Society of Chemistry.
- (C) HRT-TEM and EELS revealing Li dendrite formation at the GBs of LLZTO. Reproduced with permission from Tsai et al.<sup>75</sup> Copyright 2016, American Chemical Society.
- (D) FIB-SEM confirming the hard and hollow Li dendrite growth in the polymer solid-state electrolyte. Reproduced with permission from Golozar et al.<sup>98</sup> Copyright 2018, American Chemical Society.
- (E) AES confirming Li dendrite propagation along GBs in short-circuited  $\text{Li}/\text{LLZO}/\text{Li}$  symmetric battery. Reproduced with permission from Cheng et al.<sup>77</sup> Copyright 2017, Elsevier.
- (F) NDP revealing Li dendrite growth in  $\text{Li}/\text{LLZO}/\text{Li}$  symmetric battery. Reproduced with permission from Wang et al.<sup>99</sup> Copyright 2017, American Chemical Society.
- (G)  $^{7}\text{Li}$  NMR chemical shift image confirming Li dendrite growth within LLZTO. Reproduced with permission from Marbella et al.<sup>100</sup> Copyright 2019, American Chemical Society.
- (H) *In situ* X-ray computed tomography visualizing the process of cracks evolution of solid-state Li metal battery. Reproduced with permission from Tippens et al.<sup>78</sup> Copyright 2019, American Chemical Society.
- (I) Space X-ray diffraction tracking cracks evolution in  $\text{Li}/\text{Li}_2\text{PS}_5\text{Cl}/\text{Li}$  symmetrical batteries. Reproduced with permission from Ning et al.<sup>101</sup> Copyright 2021, Nature Publishing Group.
- (J) *In situ* microscopic showing Li dendrite formation and growth within SSEs. Reproduced with permission from Sun et al.<sup>102</sup> Copyright 2021, American Chemical Society.

**Characterizations for elucidating the causes of Li dendrites within SSEs**

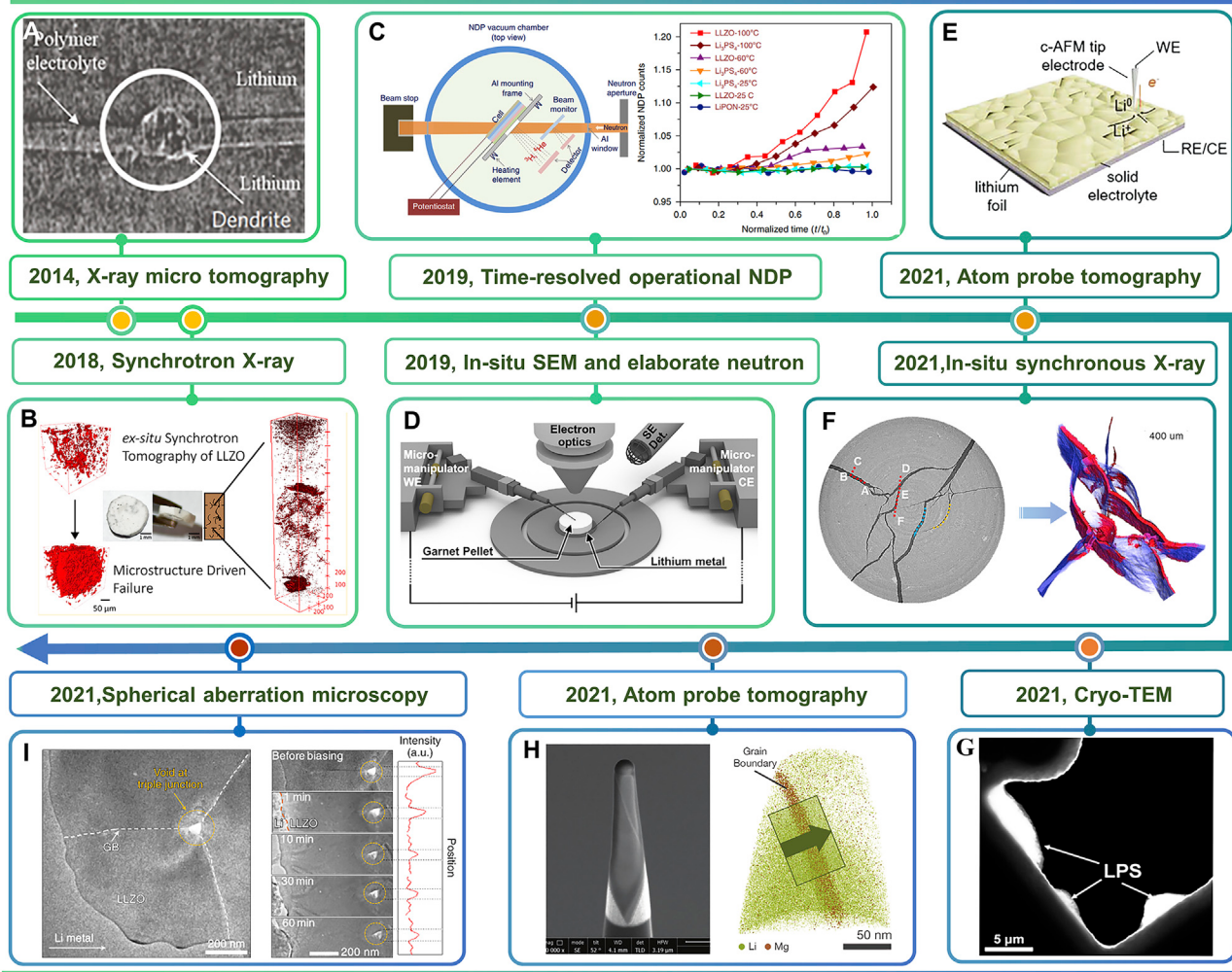


**Figure 5. Advanced characterization techniques for elucidating the causes of Li dendrites within SSEs**

- (A) X-ray micro tomography showing that the surface structure induces Li dendrites within solid polymer electrolytes. Reproduced with permission from Harry et al.<sup>104</sup> Copyright 2014, Nature Publishing Group.
- (B) Synchrotron X-ray tomography revealing that the interconnected pores accelerates Li dendrites within  $\text{Li}_x\text{La}_3\text{Zr}_2\text{O}_{12}$ . Reproduced with permission from Shen et al.<sup>105</sup> Copyright 2018, American Chemical Society.
- (C) Time-resolved operational NDP confirming that the high electrical conductivity induces Li dendrites growth within SSEs. Reproduced with permission from Han et al.<sup>89</sup> Copyright 2019, Nature Publishing Group.
- (D) *In situ* SEM and elaborate neutron showing that micro dynamics induce Li permeation in inorganic crystalline SSEs. Reproduced with permission from Krauskopf et al.<sup>107</sup> Copyright 2019, Cell Press.
- (E) c-Aonfirmingmg that GBs and inhomogeneity surface induce Li dendrites growth within ceramic SSEs. Reproduced with permission from Lu et al.<sup>108</sup> Copyright 2021, Wiley-VCH.
- (F) *In situ* synchronous X-ray computed tomography with high spatial and temporal resolution showing that Li dendrites fill in the cracks within SSEs. Reproduced with permission from Hao et al.<sup>106</sup> Copyright 2021, Elsevier.
- (G) Cryo-TEM revealing that the presence of P-based and S-based crystalline defects induces the structural cracks and short-circuit of the battery. Reproduced with permission from Sun et al.<sup>102</sup> Copyright 2021, American Chemical Society.
- (H) Atom probe tomography showing that the softening of GBs promotes the nucleation and subsequent growth of Li dendrites within SSEs. Reproduced with permission from Sina et al.<sup>109</sup> Copyright 2021, Wiley-VCH.
- (I) Spherical aberration correction electron microscopy revealing that the narrow band gap GBs provides electrons to induce Li dendrites growth within SSEs. Reproduced with permission from Liu et al.<sup>80</sup> Copyright 2021, Nature Publishing Group.

that the connective pores could reduce critical current density and accelerate Li dendrite growth within  $\text{Li}_7\text{La}_3\text{Zr}_2\text{O}_{12}$ , as shown in [Figure 5B](#).<sup>105</sup> Besides, *in situ* X-ray computed tomography, space X-ray diffraction,<sup>101</sup> and *in situ* synchrotron X-ray tomography technology<sup>106</sup> were used to demonstrate that Li dendrites grow at the crack of Li/SSEs interface and gradually penetrate into SSEs along the entire crack, eventually leading to short-circuit of the battery in [Figure 5F](#).

Furthermore, time-resolved operational NDP was used to visualize the nucleation and growth of Li dendrites within SSEs, as shown in [Figure 5C](#).<sup>89</sup> The results indicate that the high electrical conductivity of  $\text{Li}_7\text{La}_3\text{Zr}_2\text{O}_{12}$  and  $\text{Li}_3\text{PS}_4$  was the main cause of Li dendrite growth within SSEs. Moreover, conductive-atomic force microscopy (c-AFM)<sup>108</sup> in [Figure 5E](#) and atom probe tomography experiments without beam damage in [Figure 5G](#)<sup>102</sup> were used to elucidate the causes of Li dendrites within SSEs. It was shown that the GBs and heterogeneous surface of the SSEs were the dynamic characteristics and physical origin of Li dendrites growth within SSEs. In addition, cryo-transmission electron microscopy (TEM) has shown Li nucleated and propagated directly in  $\text{Li}_3\text{PS}_4$ , which was attributed to P- and S-based crystalline defects, leading to structural crack and short-circuit of the battery.

Combining equipment with the advantages of multiple characterizations should be adopted to accurately study the causes of Li dendrites within SSEs. *In situ* SEM electrodeposition with elaborate neutron measurements was used to confirm that the micro dynamics of SSEs could induce Li penetration through SSEs as shown in [Figure 5D](#).<sup>107</sup> Moreover, *in situ* high-resolution TEM and spherical aberration correction–electron microscopy equipped with valence state electron energy-loss spectroscopy were utilized to prove that electrons provided by the narrow band gap of GBs were confirmed to easily reduce  $\text{Li}^+$  to Li dendrites within SSEs, leading to short-circuit of the battery as shown in [Figure 5H](#).<sup>80</sup>

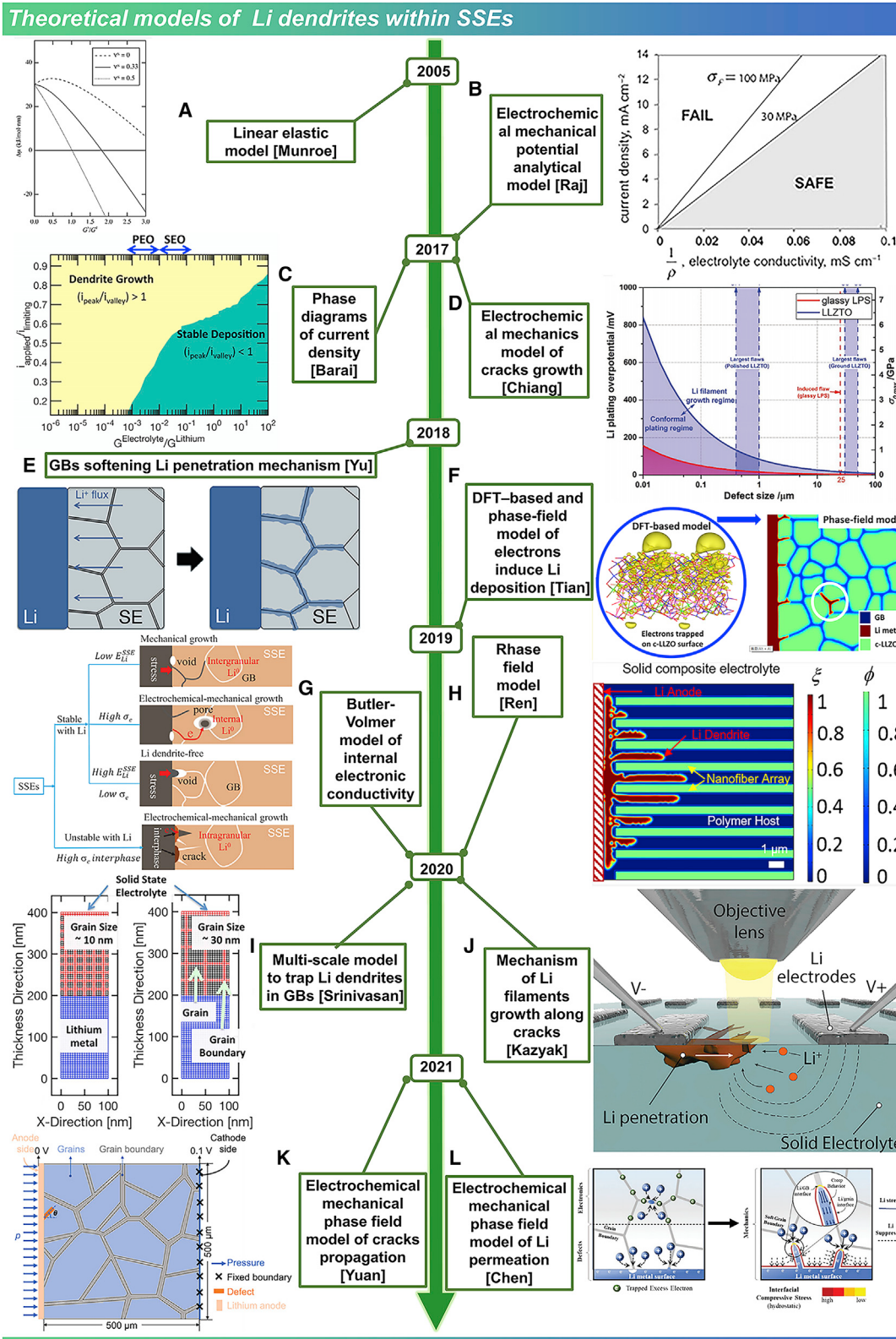
### Theoretical models

Although SSEs with high shear modulus (at least twice that of Li metal) could resist Li dendrite growth according to the Munroe's linear elastic theory model in [Figure 6A](#),<sup>70</sup> the short-circuit was still observed in solid-state batteries with high shear modulus.<sup>110</sup> Subsequently, Monroe et al. proved that the main cause of short-circuit of the battery was the internal Li dendrites within SSEs, based on space-charge-layer coupling in 2019.<sup>111</sup>

As observation has clearly shown and deeper study of Li dendrite growth within SSEs according to section 3.1 has revealed, many theoretical models have been gradually proposed to theoretically explain Li dendrite growth within SSEs. Various factors affecting the Li dendrite growth within SSEs have been studied, including grain boundaries, critical current density, pores, cracks, and electronic conductivity.

According to section 2.2, Li dendrites are easily induced through nucleation and penetration along the GBs within SSEs. As shown in [Figure 6B](#), Raj et al.<sup>112,118</sup> first proposed an analytical model based on the electrochemical-mechanical potential, which showed that the local high resistance of GBs induced the nucleation of Li dendrites. Therefore, in consideration of the effects of Li nucleation at GBs and interfacial resistance, a density-driven stabilization mechanism was developed to better predict the Li penetration within inorganic SSEs.<sup>119</sup>

Furthermore, Yu and Siegel<sup>87</sup> proposed that significant softening in elastic properties could reduce shear modulus of SSEs in nanoscale regions near GBs, resulting in



the penetration of Li dendrites within SSEs (Figure 6E). Similarly, the multiscale model was established by Srinivasan to explain that the high concentration of  $\text{Li}^+$  and the low elastic modulus in the GBs led to the high current density, resulting in Li dendrites formation within SSEs in Figure 6J.<sup>92</sup> Moreover, Chen et al.<sup>84</sup> constructed an electrochemical mechanical-phase field model, which revealed that the softening of GBs and the excess electrons in GBs induced isolated Li metal nucleation within SSEs and deeper penetration of Li dendrites along the GBs of polycrystalline  $\text{Li}_7\text{La}_3\text{Zr}_2\text{O}_{12}$  as shown in Figure 6L.

Barai et al.<sup>93,113</sup> first constructed a phase diagram to describe the relationship between the deposition of Li metal and the current density in solid polymer electrolyte in 2017, which suggested that the growth of Li dendrites was determined by critical current density (CCD) as shown in Figure 6C. Furthermore, some mechanism models in regard to the effects of Li/SSEs interface on CCD were gradually proposed.<sup>63</sup> It was manifested that the poor wettability, and lithiophobic and uneven contact of the Li/SSEs interface greatly lowered the CCD of SSEs and induced the growth of Li dendrites.<sup>120</sup>

Cracks played an important role in accelerating the penetration of Li dendrites. A model for the internal cracks of SSEs<sup>121</sup> and the reaction mechanism at the SSEs/Li interface<sup>122</sup> were reported, which verified that huge volume expansion and stress caused by Li deposition at SSEs/Li interface were the fundamental cause of the crack, leading to the Li penetration and short-circuit of the battery. Besides, Swamy et al.<sup>123</sup> constructed an electrochemical mechanical model to explain how the defect of Li/SSEs interface induced Li penetration, thus resulting in short-circuit of the battery.

As shown in Figure 6D, the electrochemical mechanical model of Li-filled cracks was first proposed to explain that Li dendrites nucleated and propagated through the brittle SSEs via Griffith-like crack extension, resulting in short-circuit of the battery.<sup>85</sup> Similarly, Kazyak et al.<sup>88</sup> verified the mechanical cracking mechanism that the infiltration of Li metal within the ceramic SSEs in 2020, which showed that the penetration rate of Li dendrites was proportional to the current density as shown in Figure 6I. Furthermore, Yuan et al.<sup>117</sup> established an electrochemical-mechanical coupled phase field model for the first time by quantitatively investigating the growth and the crack propagation of Li dendrites within SSEs, which confirmed that Li dendrites tend to grow at crack zones as shown in Figure 6K. Therefore, increasing the fracture threshold strain and fracture energy could be helpful to inhibit cracks and suppress Li dendrites within SSEs.

High relative electronic conductivity of SSEs is an important reason leading to Li dendrite growth within SSEs. Wang et al.<sup>115</sup> first proposed that Li dendrites were

---

**Figure 6. Theoretical models of Li dendrites growth within SSEs**

- (A) Munroe's linear elastic theory model. Reproduced with permission from Monroe et al.<sup>70</sup> Copyright 2005, The Electrochemical Society.
- (B) Electrochemical-mechanical potential analytical model. Reproduced with permission from Raj et al.<sup>112</sup> Copyright 2017, Elsevier.
- (C) Phase diagrams of current density. Reproduced with permission from Barai et al.<sup>113</sup> Copyright 2017, The Royal Society of Chemistry.
- (D) Electrochemical electrochemical mechanical model. Reproduced with permission from Porz et al.<sup>85</sup> Copyright 2017, Wiley-VCH.
- (E) Mechanism for softening of GBs induces Li penetration. Reproduced with permission from Yu et al.<sup>87</sup> Copyright 2018, American Chemical Society.
- (F) DFT and phase-field model. Reproduced with permission from Tian et al.<sup>114</sup> Copyright 2019, American Chemical Society.
- (G) Butler-Volmer model of internal electronic conductivity drop Li potential. Reproduced with permission from Ji et al.<sup>115</sup> Copyright 2020, Wiley-VCH.
- (H) Rhase field model. Reproduced with permission from Ren et al.<sup>116</sup> Copyright 2020, American Chemical Society.
- (I) Multi-scale model of trapping Li dendrites in GBs. Reproduced with permission from Barai et al.<sup>92</sup> Copyright 2020, The Electrochemical Society.
- (J) Mechanism of Li filaments growth along cracks. Reproduced with permission from Kazyak et al.<sup>88</sup> Copyright 2020, Cell Press.
- (K) Electrochemical mechanical phase field model. Reproduced with permission from Yuan et al.<sup>117</sup> Copyright 2021, Elsevier.
- (L) Electrochemical mechanical phase field model of Li permeation. Reproduced with permission from Tantratian et al.<sup>84</sup> Copyright 2021, Wiley-VCH.

formed within SSEs when the applied potential was greater than the critical overpotential ( $\eta^*$ ) based on the Butler-Volmer model as shown in [Figure 6G](#). Once the local electronic conductivity of SSEs is high enough, the atomic Li electrochemical potential in SSEs will drop to a potential similar to the Li plating on the anode, thus causing nucleation and growth of Li dendrites within SSEs. Density functional theory (DFT) was also used to simulate the Li nucleation tendency in  $\text{Li}_7\text{La}_3\text{Zr}_2\text{O}_{12}$  (LLZO), which showed that the trapped excess electrons were distributed around the La atoms on the LLZO surface and induced the reduction of  $\text{Li}^+$  to Li metal.<sup>124</sup> Moreover, the coupled phase field model in section 3.2.3 also shows that excessive surface electrons will affect the initial position of Li dendrites in GBs of the LLZO.

There are some other factors that could affect the growth of Li dendrites within SSEs. Ren et al.<sup>116</sup> developed a phase field model to simulate the growth of Li dendrites within composite SSEs ([Figure 6H](#)), which confirmed that the elastic modulus and the width of electrolyte nanochannel were two key factors controlling Li dendrite growth within composite SSEs. Nevertheless, Wang et al.<sup>125</sup> proved that the stacking pressure significantly influenced Li dendrite growth, crack propagation, and interface stability from the mechanical perspective by describing the Li/SSEs dynamic interface as a function of superimposed pressure and current density. It could be concluded that the high yield strength of Li metal at higher current densities reduced the initial formation time and increased the growth rate of Li dendrites by constructing a multiscale model to capture Li dendrite growth within the  $\text{Li}_7\text{La}_3\text{Zr}_2\text{O}_{12}$ .<sup>92</sup>

The growth of Li dendrites within SSEs is not controlled by a single factor but a combination of multiple factors. Qi et al.<sup>114</sup> first reported a multiscale model coupled density functional theory (DFT) calculation with the phase-field method, confirming that the internal defects, pores and GBs junction, and their electronic conducting properties could induce Li dendrites growth within SSEs in [Figure 6F](#). Furthermore, Yuan et al.<sup>126</sup> established an electrochemical coupling mechanism to comprehensively explain the Li dendrite growth within SSEs. It was indicated that the nucleation of Li dendrites started from the initial defects such as pores, voids, cracks, and GBs. Moreover, high relative electronic conductivity and insufficient critical current density provided a driving force for the growth of Li dendrites within SSEs. Finally, Li dendrites further grow and penetrate through entire SSEs, resulting in short-circuit of the battery.

## SUPPRESSING LI DENDRITES WITHIN SSEs

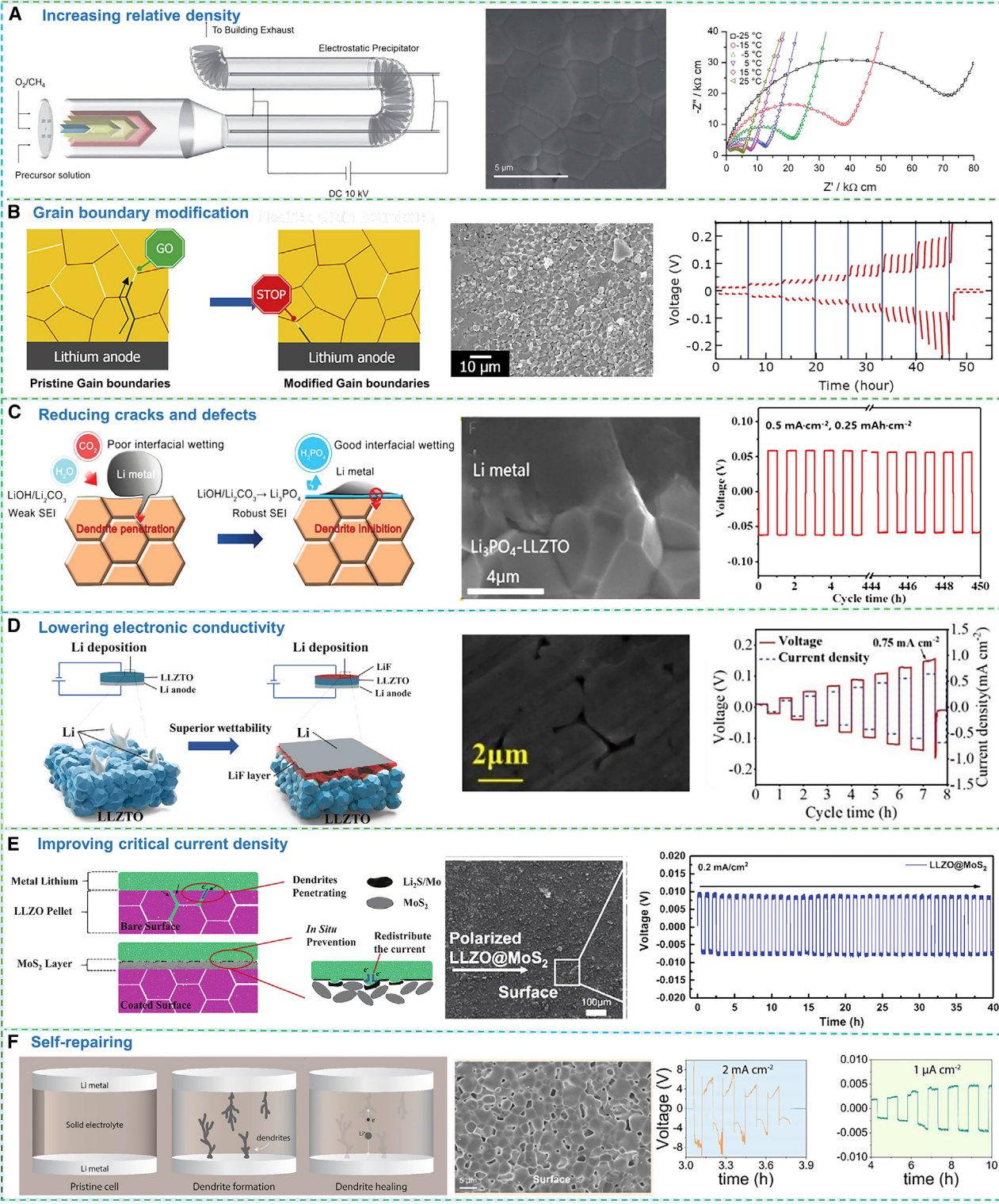
Based on the abovementioned mechanism and advanced characterizations, various strategies have been proposed to suppress Li dendrites within SSEs.

### Increasing relative density

Increasing the relative density of SSEs could directly reduce the voids and pores of SSEs, thus suppressing Li dendrites within SSEs.

Adjusting the synthesizing strategies of SSEs was proved to be an effective way to improve the relative density of SSEs. Guo et al.<sup>127</sup> prepared high relative density (96%) of  $\text{Li}_{6.75}\text{La}_3\text{Zr}_{1.75}\text{Ta}_{0.25}\text{O}_{12}$  (LLZTO) by flow oxygen sintering process for the first time. The oxygen filling and lattice diffusion could effectively remove the pores near the grain boundary via optimization of the sintering atmosphere. Similarly, Yamada et al.<sup>128</sup> obtained 96% of the relative density of LLZTO by using the spark plasma technique as shown in [Figure 7A](#). Moreover, the casting–sintering

## Suppressing Li dendrites within SSEs



technique<sup>129</sup>, cold isostatic pressing technique<sup>130</sup>, rapid induction hot pressing technique<sup>131</sup> and uniaxial hot-pressing sintering technique<sup>132</sup> were also confirmed to improve relative density by integrating GBs and reducing the pores and voids of SSEs.

Introducing doping elements and oxide into SSEs is another effective way to increase relative density of SSEs. Murugan et al.<sup>137</sup> adopted hot isostatic post-sintering technology to prepare Al-doped  $\text{Li}_7\text{La}_3\text{Zr}_2\text{O}_{12}$  with a high relative density of 98%, by adding 1 wt.%  $\text{Li}_4\text{SiO}_4$ , which could enhance the integrity of GBs and minimize pores. Similarly, Ta-substituted<sup>75</sup> and  $\text{Al}_2\text{O}_3$ -doped  $\text{Li}_7\text{La}_3\text{Zr}_2\text{O}_{12}$ <sup>57</sup> also achieved a high relative density (more than 99%) by hot press sintering.

### Grain boundary modification

Previous studies suggested that the short-circuit of the battery is due to Li dendrite growth within SSEs brought by Li nucleation and permeation along GBs, so GB modification and other strategies were proposed to completely suppress Li dendrites.<sup>138</sup>

Surface treatments could effectively inhibit Li dendrite growth along GBs and avoid the direct contact between Li metal and GBs. Tsai et al.<sup>75</sup> polished the surface of  $\text{Li}_{6.75}\text{La}_3\text{Zr}_{1.75}\text{Ta}_{0.25}\text{O}_{12}$  and introduced an Au buffer layer, which improved ionic conductivity of GBs and adjusted Li/SSEs interface to inhibit Li dendrite growth at GBs. Similarly, coating a thin  $\text{Li}^+$  conducting polymer<sup>139</sup> and introducing a Li-Ag alloy layer on ceramic SSE interfaces were also used to modify GBs and suppress Li dendrites at GBs.<sup>140</sup>

Some additives were also helpful to adjust the structure of GBs and inhibit Li dendrite growth along, and penetration of GBs. Yamada et al.<sup>65</sup> introduced  $\text{Li}_2\text{CO}_3$  and  $\text{LiOH}$  in  $\text{Li}_{6.75}\text{La}_3\text{Zr}_{1.75}\text{Ta}_{0.25}\text{O}_{12}$ (LLZTO) to modify GBs and inhibit the growth of Li dendrites along GBs by improving the interconnection between grains in Figure 7B. Furthermore, adding  $\text{Li}_6\text{Zr}_2\text{O}_7$  in LLZTO to decompose into  $\text{Li}_2\text{ZrO}_3$  during the sintering process<sup>141</sup> and introducing lithophilic  $\text{Li}_3\text{OCl}$  into the GBs of LLZTO were useful to fill in the gap between grains and enhance intergrain bonding, thus inhibiting Li dendrites growth along GBs.<sup>76</sup>

Besides, the direct reduction of GBs could alleviate Li dendrite growth and delay short-circuited time. Kataoka et al. adopted the floating zone method to prepare a garnet type  $\text{Li}_{6.5}\text{La}_3\text{Zr}_{1.5}\text{Nb}_{0.5}\text{O}_{12}$  without GBs and pores.<sup>142</sup> Moreover, ionic liquid with high ionic conductivity was investigated as to its potential to inhibit Li dendrite growth along GBs through filling the voids within the  $\text{Li}_7\text{La}_3\text{Zr}_2\text{O}_{12}$  and coterminous GBs.

### Reducing cracks and defects

Li dendrites nucleate at the cracks and defects of SSEs, and propagate through entire SSEs, resulting in short-circuit of the battery. Therefore, it is necessary to

---

### Figure 7. Suppressing Li dendrites within SSEs

- (A) Increasing relative density of SSEs. Reproduced with permission from Yi et al.<sup>129</sup> Copyright 2016, The Royal Society of Chemistry.
- (B) Grain boundary modification. Reproduced with permission from Hongahally et al.<sup>65</sup> Copyright 2017, Elsevier.
- (C) Reducing cracks and defects to suppress Li penetration. Reproduced with permission from Ruan et al.<sup>133</sup> Copyright 2019, The Royal Society of Chemistry.
- (D) Lowering electron conductivity of SSEs. Reproduced with permission from Tang et al.<sup>134</sup> Copyright 2020, The Royal Society of Chemistry.
- (E) Improving CCD of SSEs. Reproduced with permission from Fu et al.<sup>135</sup> Copyright 2019, The Royal Society of Chemistry.
- (F) Self-repairing of Li dendrites within SSEs. Reproduced with permission from Parejija et al.<sup>136</sup> Copyright 2020, American Chemical Society.

reduce cracks and defects for inhibiting Li dendrite penetration within SSEs. The introduction of artificial interface layer and mechanical filling, and the construction of multilayer SSEs are the main strategies.

Artificial interface layer, with good ionic conductivity, good wettability, electrical insulation, and high mechanical strength was helpful in inhibiting cracks and defects.<sup>143</sup> Wen et al.<sup>133</sup> constructed Li<sub>3</sub>PO<sub>4</sub> layers on the surface of the Li<sub>6.75</sub>La<sub>3</sub>Zr<sub>1.75</sub>Ta<sub>0.25</sub>O<sub>12</sub> as shown in Figure 7C. It was shown that the Li<sub>3</sub>PO<sub>4</sub> layer not only promoted interfacial wettability, but also provided robust interfacial phase, thus reducing the cracks and defects to inhibit Li penetration. Furthermore, a LiPON,<sup>96</sup> ZnO,<sup>144</sup> Al<sub>2</sub>O<sub>3</sub> coating layer and Li<sub>1.3</sub>Al<sub>0.3</sub>Ti<sub>1.7</sub>(PO<sub>4</sub>)<sub>3</sub> composite polymer coating layer<sup>66</sup> on the interface of SSEs could also effectively reduce cracks and defects to inhibit Li dendrites penetration.<sup>145</sup>

Mechanical filling was another effective strategy to inhibit cracks and Li penetration. Wang et al.<sup>146</sup> filled perfluoromethoxy butane (HFE) into the voids of Li<sub>7</sub>P<sub>3</sub>S<sub>11</sub>. Once Li penetrated into Li<sub>7</sub>P<sub>3</sub>S<sub>11</sub>, HFE preferential reacted with Li metal and formed LiF interface within SSEs, which consumed Li metal and inhibited Li dendrite penetration within SSEs. Moreover, introducing Ti<sup>4+</sup> in Li<sub>6.75</sub>La<sub>3</sub>Zr<sub>1.75</sub>Ta<sub>0.25</sub>O<sub>12</sub>,<sup>64</sup> filling garnet particles into polymer matrix,<sup>53</sup> and adding silicon nanoparticles in the micropores of Li<sub>7</sub>La<sub>3</sub>Zr<sub>2</sub>O<sub>12</sub> effectively reduced defects and cracks to inhibit Li dendrite penetration.<sup>81</sup>

Multilayer SSEs could combine the mechanical properties of ceramics with the flexibility of polymers, thus inhibiting Li penetration. Pervez et al.<sup>147</sup> effectively prevented Li penetration by synthesizing a flexible and mechanically robust polymer film, which consisted of Li perchlorate and garnet particles as an intermediate layer. In addition, the introduction of sandwich-structured SSEs, such as those produced by adding stable Li<sub>5.5</sub>PS<sub>4.5</sub>Cl<sub>1.5</sub> on both surfaces of unstable Li<sub>10</sub>Ge<sub>1</sub>P<sub>2</sub>S<sub>12</sub>,<sup>148</sup> polymer/ceramic/polymer sandwich electrolytes,<sup>149</sup> and sandwich-type composite SSEs (ceramic-in-polymer or polymer-in-ceramic)<sup>150</sup> could effectively suppress Li penetration, thus achieving dendrite-free SSEs.

### Lowering electronic conductivity

High local electronic conductivity would directly reduce the overpotential of Li nucleation within SSEs and induce Li dendrite growth in the interior of SSEs.<sup>89</sup> Therefore, it is necessary to lower electronic conductivity of SSEs.

Introducing an electronic insulating layer is effective in lowering the electronic conductivity of SSEs, especially at GBs. Based on the insulating property of LiF, Tang et al.<sup>134</sup> prepared ultra-thin LiF layers with controllable thickness by vacuum evaporation deposition, which reduced the electrical conductivity on the GBs in Li<sub>6.75</sub>La<sub>3</sub>Zr<sub>1.75</sub>Ta<sub>0.25</sub>O<sub>12</sub> (Figure 7D). Moreover, a coating LiAlO<sub>2</sub> layer on the GBs of Li<sub>7</sub>La<sub>2.75</sub>Ca<sub>0.25</sub>Zr<sub>1.75</sub>Nb<sub>0.25</sub>O<sub>12</sub> could also effectively lower the electronic conductivity at GBs and thus inhibit Li dendrites growth within SSEs.<sup>90</sup>

Electronic insulation additives could effectively lower the electronic conductivity of SSEs. Sun et al.<sup>67</sup> added electrically insulated LiF into the SSEs to prevent contact between electrons and Li<sup>+</sup>, thus inhibiting Li dendrite nucleation within SSEs. Although LiF possessed high interfacial energy and low electronic conductivity, insufficient ionic conductivity hindered uniform Li<sup>+</sup> transport. Therefore, simply coating LiF on SSEs could not effectively inhibit Li dendrite growth. Based on this, Wang et al.<sup>115</sup> inserted Li<sub>3</sub>N with high ionic conductivity between LiF particles to

**Table 1. Summary of strategies for improving critical current density in the recent literatures**

Electrolyte	Modified strategy	Initial CCD ( $\text{mA cm}^{-2}$ )	Modified CCD ( $\text{mA cm}^{-2}$ )	Year and Ref.
$\text{Li}_{6.5}\text{La}_3\text{Zr}_{1.5}\text{Ta}_{0.5}\text{O}_{12}$	Au buffer layer	0.15 at 25°C	0.5 at 25°C	2016 and 68
$\text{Li}_{2\text{S}-\text{P}2\text{S}5}$	Hot-press at 170°C	0.5 at 25°C	1 at 25°C	2017 and 150
$\text{Li}_{6.5}\text{La}_3\text{Zr}_{1.5}\text{Ta}_{0.5}\text{O}_{12}$	$\text{Li}_2\text{CO}_3$ and LiOH	0.15 at 25°C	0.6 at 25°C	2017 and 126
$\text{Li}_{7-x}\text{La}_3\text{Zr}_{2-x}\text{Nb}_x\text{O}_{12}$	Floating zone method	0.15 at 25°C	0.5 at 25°C	2018 and 129
$\text{Li}_2\text{S}-\text{P}_2\text{S}_5$	Dope LiI	2.4 at 100°C	3.9 at 100°C	2018 and 146
$\text{Li}_7\text{La}_3\text{Zr}_2\text{O}_{12}$	Ga-doped	0.15 at 25°C	0.3 at 25°C	2018 and 151
$\text{LiBH}_4$	Add LiF	2.8 at 125°C	6.6 at 125°C	2019 and 66
$\text{Li}_7\text{La}_3\text{Zr}_2\text{O}_{12}$	Coate MoS <sub>2</sub> layer	0.7 at 100°C	2.2 at 100°C	2019 and 152
$\text{Li}_{6.5}\text{La}_3\text{Zr}_{1.5}\text{Ta}_{0.5}\text{O}_{12}$	Form $\text{Li}_3\text{PO}_4$ layer	0.15 at 25°C	0.8 at 25°C	2019 and 131
$\text{Li}_7\text{La}_{2.75}\text{Ca}_{0.25}\text{Zr}_{1.75}\text{Nb}_{0.25}\text{O}_{12}$	Coate $\text{AlO}_2$ layer	0.4 at 25°C	0.75 at 25°C	2019 and 78
$\text{Li}_{6.5}\text{La}_3\text{Zr}_{1.5}\text{Ta}_{0.5}\text{O}_{12}$	Add $\text{Li}_4\text{SiO}_4$ and HIP	0.12 at 25°C	0.4 at 25°C	2020 and 148
$\text{Li}_7\text{La}_3\text{Zr}_2\text{O}_{12}$	$\text{Li}_3\text{N}/\text{Cu}$ layer	0.15 at 25°C	1.2 at 25°C	2020 and 154
$\text{Li}_{6.5}\text{La}_3\text{Zr}_{1.5}\text{Ta}_{0.5}\text{O}_{12}$	Add $\text{Li}_{2.3}\text{C}_{0.7}\text{B}_{0.3}\text{O}_3$	0.15 at 25°C	0.3 at 25°C	2020 and 149
$\text{Li}_6\text{PS}_5\text{Cl}$	$\text{Li}_3\text{N}$ replaces $\text{Li}_2$	0.89 at 25°C	1.52 at 25°C	2021 and 147
$\text{Li}_{6.5}\text{La}_3\text{Zr}_{1.5}\text{Ta}_{0.5}\text{O}_{12}$	$\text{Li}_2\text{O}$ layer	0.15 at 25°C	1.1 at 25°C	2021 and 153
PEO-LiTFSI	Mg( $\text{ClO}_4$ ) <sub>2</sub> additive	0.3 at 55°C	1.6 at 55°C	2021 and 39
PEO	Add $\text{Li}_2\text{S}_6$	0.15 at 40°C	0.9 at 40°C	2021 and 145
$\text{Li}_{6.5}\text{La}_3\text{Zr}_{1.5}\text{Ta}_{0.5}\text{O}_{12}$	Add $\text{Li}_6\text{Zr}_2\text{O}_7$	0.15 at 25°C	1.4 at 25°C	2021 and 127

prepare a composite electrolyte, which inhibited the growth of Li dendrites within  $\text{Li}_3\text{PS}_4$ .

In addition, blocking electrons from entering SSEs was another useful way to inhibit the internal growth of Li dendrites. Tian et al.<sup>124</sup> preset an  $\text{Li}_2\text{PO}_2\text{N}$  interlayer on the  $\text{Li}/\text{Li}_7\text{La}_3\text{Zr}_2\text{O}_{12}$  interface, which could cut off the electronic pathway for the formation of the Li metal, thus suppressing Li dendrites within SSEs. What is more, laser annealing was performed on the surface of  $\text{Li}_{6.75}\text{La}_3\text{Zr}_{1.75}\text{Ta}_{0.25}\text{O}_{12}$ (LLZTO) to obtain an amorphous LLZTO- $\text{Li}_2\text{O}_2$  composite layer, thus effectively preventing electrons flowing into the GBs.<sup>79</sup>

### Improving critical current density

According to section 2.4, critical current density (CCD) reflected the ability of SSEs to suppress Li dendrites in the interior of SSEs.<sup>151</sup> The related methods of improving CCD of SSEs are listed in Table 1.<sup>67</sup>

Sakamoto et al.<sup>131</sup> proposed that interface stability and dynamics are dependent on variables of temperature and current density. It was found that increasing working temperature of the battery by rapid hot-pressing technique could effectively improve CCD (from 0.2  $\text{mA cm}^{-2}$  at 70°C to 3.5  $\text{mA cm}^{-2}$  at 160°C) of polycrystalline  $\text{Li}_7\text{La}_3\text{Zr}_2\text{O}_{12}$ .

Dopants played an important role in improving CCD of SSEs. Goodenough et al.<sup>152</sup> used  $\text{Li}_2\text{S}_6$  as an additive for polyethylene oxide-based SSEs, and thus formed a stable and uniform  $\text{Li}_2\text{S}/\text{Li}_2\text{S}_2$  layer that inhibited Li dendrite growth within SSEs. Moreover,  $\text{Li}^+$  in  $\text{Li}_2\text{S}_6$  strongly interacted with  $\text{O}^{2-}$  in polyethylene oxide-based SSEs, which reduced the formation of microcrystals in SSEs and improved the CCD from 0.2 to 0.9  $\text{mA cm}^{-2}$ . In addition, electronic insulative additives with high ionic conductivity, such as LiI,<sup>153</sup>  $\text{Li}_3\text{N}$ ,<sup>68</sup> and LiF<sup>67</sup> could also increase the CCD of SSEs. Besides, adding  $\text{Li}_4\text{SiO}_4$  in Al-doped  $\text{Li}_7\text{La}_3\text{Zr}_2\text{O}_{12}$  by hot isostatic pressing,<sup>154</sup> adding  $\text{Li}_{2.3}\text{C}_{0.7}\text{B}_{0.3}\text{O}_3$  into  $\text{Li}_{6.75}\text{La}_3\text{Zr}_{1.75}\text{Ta}_{0.25}\text{O}_{12}$ <sup>155</sup> and adding Mg( $\text{ClO}_4$ )<sub>2</sub> additive into PEO-based SSEs<sup>41</sup> could improve the stability of the Li/SSEs interface, thus effectively increasing the CCD of SSEs.

Structural optimization is also capable of bettering CCD of SSEs. Sakamoto et al.<sup>156</sup> optimized the atomic/microstructure of SSEs by hot-press at 170°C, elevating the CCD of Li<sub>2</sub>S-P<sub>2</sub>S<sub>5</sub> from 0.5 to 1 mA cm<sup>-2</sup> at room temperature. Moreover, Ga-doped Li<sub>7</sub>La<sub>3</sub>Zr<sub>2</sub>O<sub>12</sub>(LLZO) was prepared to improve the stability of cubic garnet electrolytes and avoid the initial propagation of Li metal in the GBs, thus increasing the CCD of LLZO.<sup>157</sup> Effective methods to increase CCD includes increasing the dielectric constant, reducing the grain size, increasing the surface energy of the Li/SSEs interface, reducing the interfacial dynamic resistance, and decreasing the interfacial capacitance.<sup>111</sup>

In addition, coating mechanically stable layers such as MoS<sub>2</sub><sup>135</sup>, Li<sub>2</sub>CO<sub>3</sub>, and LiOH<sup>65</sup> could effectively increase the CCD of SSEs by reducing voids and improving the interconnection between grains as shown in Figure 7E. Pan et al.<sup>158</sup> designed a Li<sub>2</sub>O lithiophilic interface layer on Li<sub>6.75</sub>La<sub>3</sub>Zr<sub>1.75</sub>Ta<sub>0.25</sub>O<sub>12</sub> (LLZTO) surface to improve the wettability of LLZTO/Li metal interface, which effectively inhibited Li penetration and improved the CCD from 0.5 to 1.1 mA cm<sup>-2</sup> at 25°C. Besides, coating a Li<sub>3</sub>N/Cu hybrid conductive layer on LLZTO could also effectively improve the CCD from 0.1 to 1.2 mA cm<sup>-2</sup> at room temperature.<sup>159</sup>

#### Other means

In addition to the above strategies, there are many other ways to suppress Li dendrites within SSEs. Hu et al.<sup>69</sup> adopted *in situ* neutron depth analysis, and elucidated that short-circuit of the battery caused by Li dendrites growth in garnet-based SSEs was a reversible condition. It was found that the deposited Li-rich phase was consumed by the chemical reaction of the cathode or local garnet matrix, and short-circuit of the battery would be completely or partially terminated under rest or subjected to a discharge current. Therefore, Amin et al.<sup>136</sup> developed an *in situ* electrochemical self-repairing method by introducing a small current, which could remove Li dendrites from the bulk phase of Li<sub>6.75</sub>La<sub>3</sub>Zr<sub>1.75</sub>Ta<sub>0.25</sub>O<sub>12</sub> as shown in Figure 7F.

According to previous reported studies, stable solid electrolyte interphase (SEI) could effectively inhibit Li dendrite growth at the interface of Li/solid-state electrolytes.<sup>16,18</sup> Recent studies start to concentrate on building stable SEI to inhibit Li dendrite penetration through SSEs. By comparing the origin and evolution of Li dendrite growth within Li<sub>6.1</sub>Ga<sub>0.3</sub>La<sub>3</sub>Zr<sub>2</sub>O<sub>12</sub> (LLZO) and Li<sub>2</sub>O-Al<sub>2</sub>O<sub>3</sub>-P<sub>2</sub>O<sub>5</sub>-TiO<sub>2</sub>-GeO<sub>2</sub> (LATP),<sup>81</sup> Wu et al.<sup>160</sup> studied the failure mechanism of solid-state batteries and demonstrated the significance of SEI in preventing Li dendrite permeation through SSEs. Furthermore, they used Si nanoparticles to fill the surface micropores of LLZO and formed a stable SEI to inhibit Li dendrite penetration. Additionally, other similar solid electrolyte interphases such as Li<sub>1</sub><sup>153</sup>, Li<sub>3</sub>N,<sup>68</sup> and LiF<sup>161</sup> were found to be useful in inhibiting Li dendrite penetration through SSEs.

Moreover, the yield strength of Li metal played an effect on forming time and growth rate of Li dendrites.<sup>92</sup> Therefore, increasing the yield strength of SSEs could increase the elastic modulus, thus inhibiting Li dendrite growth within SSEs.

#### SUMMARY AND OUTLOOK

Utilizing nonflammable inorganic solid-state electrolytes (SSEs) holds great promise for preventing dendrite growth and achieving safe all-solid-state Li metal batteries. However, Li dendrites may still exist in the interior of inorganic SSEs and impede their practical application. This review provides a systematic understanding of Li

**Table 2.** Brief summary of the causes of Li dendrites within SSEs and corresponding suppression strategies

Causes of Li dendrites	Suppression strategies	Specific methods
Voids and pores	Increasing relative density	<ul style="list-style-type: none"> <li>● Adjusting strategies of synthesizing SSEs such as spark plasma technique.</li> <li>● Introducing doping elements and oxide into SSEs such as Ta and <math>\text{Al}_2\text{O}_3</math>.</li> </ul>
Grain boundaries	Modifying grain boundaries	<ul style="list-style-type: none"> <li>● Surface treatments such as Au buffer layer and Li ion conduct polymer.</li> <li>● Adding additives such as <math>\text{Li}_6\text{Zr}_2\text{O}</math> and <math>\text{Li}_3\text{OCl}</math>.</li> <li>● Directly reduction of GBs such as floating zone method.</li> </ul>
Cracks and defects	Reducing cracks and defects	<ul style="list-style-type: none"> <li>● Artificial interface layer such as LiPON and ZnO.</li> <li>● Mechanical filling like <math>\text{Li}_7\text{P}_3\text{S}_{11}</math> and Si nanoparticles.</li> <li>● Multilayer SSEs such as sandwich electrolyte.</li> </ul>
High relative electronic conductivity	Lowering electronic conductivity	<ul style="list-style-type: none"> <li>● Introducing electronic insulating layer such as LiF and <math>\text{LiAlO}_2</math>.</li> <li>● Electronic insulation additives such as <math>\text{Li}_3\text{N}\text{-LiF}</math>.</li> <li>● Blocking electrons from entering SSEs for example <math>\text{Li}_2\text{PO}_2\text{N}</math> interlayer.</li> </ul>
Lower critical current density	Improving critical current density	<ul style="list-style-type: none"> <li>● Increasing cycle temperature for example rapid induction hot pressing.</li> <li>● Adding dopants such as <math>\text{Li}_2\text{S}_6</math> and <math>\text{LiI}</math>.</li> <li>● Structural optimization such as reduce grain size and reduce resistance.</li> <li>● Coating a mechanically stable layers such as <math>\text{MoS}_2</math> and <math>\text{Li}_4\text{SiO}_4</math>.</li> </ul>
Other factors	Self-repairing	<ul style="list-style-type: none"> <li>● Self-repairing like introduce small current repair.</li> <li>● Forming stable solid electrolyte interphase.</li> <li>● Increasing yield strength.</li> </ul>

dendrite growth in the interior of inorganic SSEs. Combining with advanced characterization techniques and theoretical calculations, theoretical models of Li dendrite growth within SSEs is elucidated in detail, and the main causes of Li dendrites growth within SSEs are further clarified. Furthermore, the corresponding strategies of suppressing Li dendrites are comprehensively summarized (Table 2).

Based on the summary above, Li dendrite growth within SSEs is controlled by multi-faceted factors. First, the nucleation of Li dendrites started from the initial defects such as pores, voids, cracks, and GBs. Moreover, high relative electronic conductivity and insufficient critical current density provide a driving force for Li dendrite growth within SSEs. Finally, Li dendrites further grow along cracks and penetrate through SSEs, resulting in short-circuit of the battery. Accordingly, various strategies to suppress Li dendrites mainly include: (1) increasing relative density to reduce voids and pores, (2) modifying GBs to inhibit Li dendrites nucleation at GBs, (3) reducing cracks and defects to prevent Li penetration, and (4) improving CCD and lowering electron conductivity to inhibit Li dendrites formation. Furthermore, self-repairing and other strategies are also proven methods to suppress Li dendrites within SSEs.

Although there are numerous strategies for modifying SSEs, there is still no comprehensive strategy to completely suppress Li dendrites. Therefore, we recommend that in future research, more accurate theoretical calculations are needed to reveal

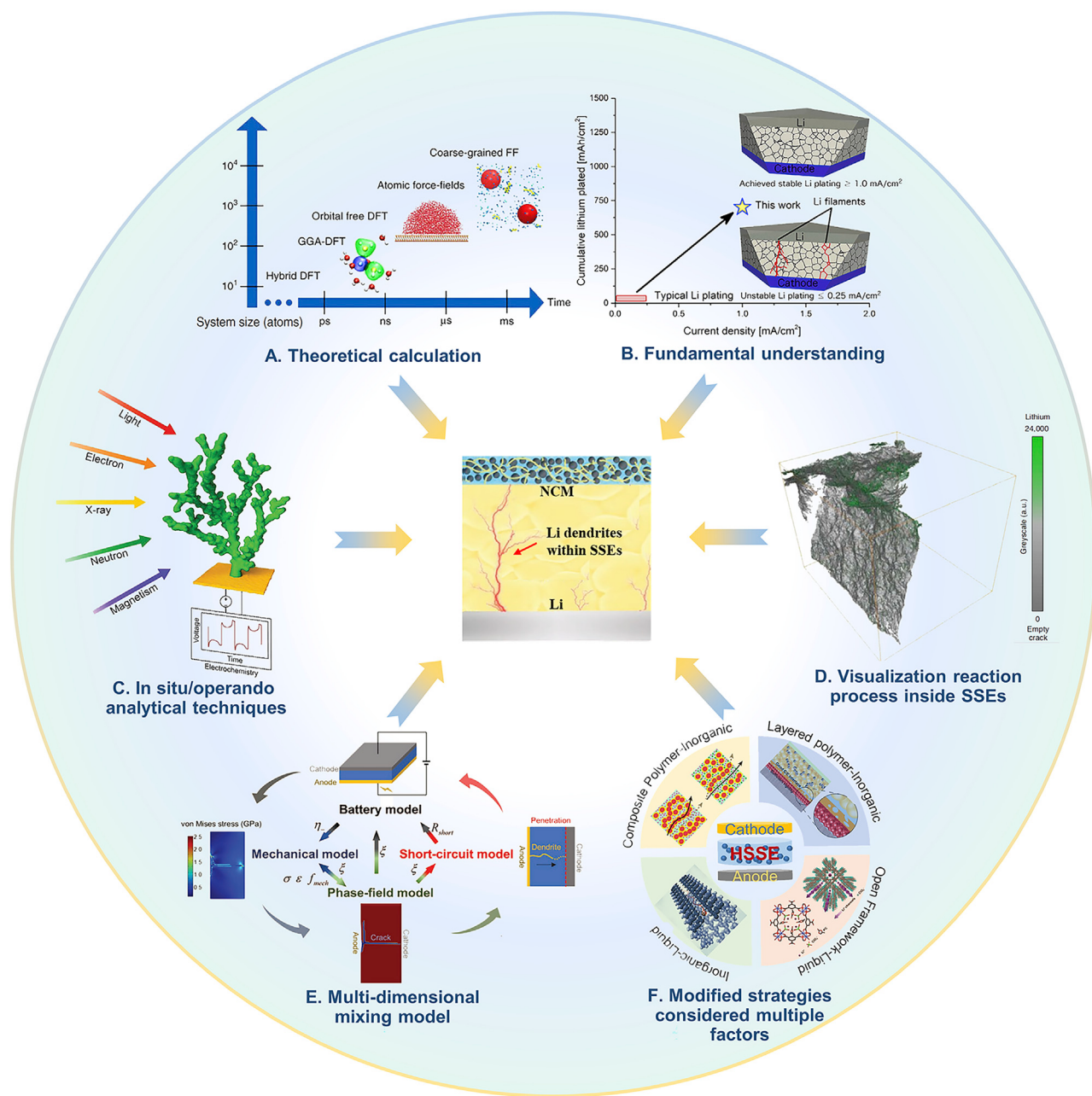


**Figure 8. Outlook for future research of suppressing Li dendrites within SSEs**

(A) Theoretical calculation. Reproduced with permission from Lukatskaya et al.<sup>162</sup> Copyright 2016, Nature Publishing Group.

(B) Fundamental understanding. Reproduced with permission from Taylor et al.<sup>163</sup> Copyright 2018, Elsevier.

(C) In situ/operando analytical techniques. Reproduced with permission from Um et al.<sup>164</sup> Copyright 2020, Wiley-VCH.

(D) Visualization of reaction process within SSEs. Reproduced with permission from Ning et al.<sup>101</sup> Copyright 2021, Nature Publishing Group. (E) Multi-dimensional mixing model. Reproduced with permission from Yuan et al.<sup>126</sup> Copyright 2021, Wiley-VCH. (F) Modified strategies considered multiple factors. Reproduced with permission from Liu et al.<sup>165</sup> Copyright 2021, Wiley-VCH.

the causes of Li dendrites within SSEs (such as shown in Figure 8). Moreover, deepening fundamental understanding, using accurate *in situ*/operational analysis techniques and constructing multidimensional mixing models combined with multiple factors are conducive to study the causes of Li dendrite growth in the interior of SSEs, thus providing possible pathways for effectively suppressing Li dendrites.

In addition, modified strategies that consider multiple causes of Li dendrites within SSEs are urgently needed. Based on the above analysis, we believe that the combination of organic SSEs and inorganic SSEs can make use of their respective advantages. On the one hand, organic SSEs can eliminate pores, voids, cracks and GBs of the Li/SSEs interface. On the other hand, inorganic SSEs can effectively improve ionic conductivity and reduce electronic conductivity of the composite SSEs. Through such combinations, the industrialization of the dendrite-free all-solid-state Li metal batteries with high-energy density is just around the corner.

## ACKNOWLEDGMENTS

This work was supported by the National Natural Science Foundation of China (Grant Nos. 51874110 and 51604089), Natural Science Foundation of Heilongjiang Province (YQ2021B004), and Open Project of State Key Laboratory of Urban Water Resource and Environment (Grant No QA202138).

## AUTHOR CONTRIBUTIONS

Conceptualization, B.W., D.W., and S.D.; Investigation, Q.L., Y.J., B.W., Y.C., F.J., B.W., H.R., and N.Z.; Writing—Original Draft, Q.L., Y.J., and B.W.; Writing—Review and Editing, B.W., R.X., Y.L., T.Z., Y.Z., H.L., and S.D.; Funding Acquisition, B.W., and D.W.; Supervision, B.W., and D.W.

## DECLARATION OF INTERESTS

The authors declare no competing interests.

## REFERENCES

- Whittingham, M.S. (1976). Electrical energy storage and intercalation chemistry. *Science* 192, 1126–1127.
- Fouchard, D., and Taylor, J.B. (1987). The molcel rechargeable lithium system Multicell aspects. *J. Power Sources* 21, 195–205.
- Brandt, K., and Laman, F.C. (1989). Reproducibility and reliability of rechargeable lithium-molybdenum disulfide batteries. *J. Power Sources* 25, 265–276.
- Brandt, K. (1994). Historical development of secondary lithium batteries. *Solid State Ion.* 69, 173–183.
- Fouchard, D., and Lechner, L. (1993). Analysis of safety and reliability in secondary lithium batteries. *Electrochim. Acta* 38, 1193–1198.
- Mizushima, K., Jones, P.C., Wiseman, P.J., and Goodenough, J.B. (1980).  $\text{Li}_x\text{CoO}_2$  ( $0 < x < 1$ ): A new cathode material for batteries of high energy density. *Mat. Research Buletin.* 15, 783–789.
- Yoshino, A. (2012). The birth of the lithium-ion battery. *Angew. Chem. Int. Ed. Engl.* 51, 5798–5800.
- Song, R.S., Ge, Y.Q., Wang, B., Lv, Q., Wang, F., Ruan, T.T., Wang, D.L., Dou, S.X., and Liu, H.K. (2019). A new reflowing strategy based on lithiophilic substrates towards smooth and stable lithium metal anodes. *J. Mater. Chem. A.* 7, 18126–18134.
- Pachhi, A.K., Nanjundaswamy, K.S., and Goodenough, J.B. (1997). Phospho-olivines as positive-electrode materials for rechargeable lithium batteries. *J. Electrochem. Soc.* 144, 1188–1194.
- Liu, Zhaolin, Aishui, Y.A., Jim, Y., and Lee, B. (1999). Synthesis and characterization of  $\text{LiNi}_{1-x}\text{Co}_x\text{Mn}_2\text{O}_4$  as the cathode materials of secondary lithium batteries. *J. Power Sources* 81–82, 416–419.
- Lin, D., Liu, Y., and Cui, Y. (2017). Reviving the lithium metal anode for high-energy batteries. *Nat. Nanotechnol.* 12, 194–206.
- Liu, T., Chu, Q., Yan, C., Zhang, S., Lin, Z., and Lu, J. (2019). Interweaving 3D network binder for high-area-capacity Si anode through combined hard and soft polymers. *Adv. Energy Mater.* 9, 1802645.
- Tarascon, J.-M., and Armand, M. (2001). Issues and challenges facing rechargeable lithium batteries. *Nature* 414, 359–367.
- Xu, W., Wang, J., Ding, F., Chen, X., Nasibulin, E., Zhang, Y., and Zhang, J.-G. (2014). Lithium metal anodes for rechargeable batteries. *Energy Environ. Sci.* 7, 513–537.
- Cheng, X.B., Zhang, R., Zhao, C.Z., and Zhang, Q. (2017). Toward safe lithium metal anode in rechargeable batteries: A review. *Chem. Rev.* 117, 10403–10473.
- Meyerson, M.L., Papa, P.E., Heller, A., and Mullins, C.B. (2021). Recent developments in dendrite-free lithium-metal deposition through tailoring of micro- and nanoscale artificial coatings. *ACS Nano* 15, 29–46.
- Cheng, X.B., Zhang, R., Zhao, C.Z., Wei, F., Zhang, J.G., and Zhang, Q. (2015). A review of solid electrolyte interphases on lithium metal anode. *Adv. Sci. (Weinh.)* 3, 1500213.
- Yu, Z., Cui, Y., and Bao, Z. (2020). Design principles of artificial solid electrolyte interphases for lithium-metal anodes. *Cell Rep. Phys. Sci.* 1, 100119.
- Jiang, Y., Wang, B., Liu, P., Wang, B., Zhou, Y., Wang, D., Liu, H., and Dou, S. (2020). Modified solid-electrolyte interphase toward stable Li metal anode. *Nano Energy* 77, 105308.
- Sun, Y., Liu, N., and Cui, Y. (2016). Promises and challenges of nanomaterials for lithium-based rechargeable batteries. *Nat. Energy* 1, 16071.
- Zhang, R., Li, N.W., Cheng, X.B., Yin, Y.X., Zhang, Q., and Guo, Y.G. (2017). Advanced micro/nanostructures for lithium metal anodes. *Adv. Sci. (Weinh.)* 4, 1600445.
- Yun, J., Park, B.K., Won, E.S., Choi, S.H., Kang, H.C., Kim, J.H., Park, M.S., and Lee, J.W. (2020). Bottom-up lithium growth triggered by interfacial activity gradient on porous framework for lithium-metal anode. *ACS Energy Lett.* 5, 3108–3114.
- Haregewoin, A.M., Wotango, A.S., and Hwang, B.-J. (2016). Electrolyte additives for lithium ion battery electrodes: Progress and perspectives. *Energy Environ. Sci.* 9, 1955–1988.
- Zhang, H., Eshetu, G.G., Judez, X., Li, C., Rodriguez-Martinez, L.M., and Armand, M. (2018). Electrolyte additives for lithium metal anodes and rechargeable lithium metal

- batteries: Progress and perspectives. *Angew. Chem. Int. Ed. Engl.* 57, 15002–15027.
25. Jie, Y., Ren, X., Cao, R., Cai, W., and Jiao, S. (2020). Advanced liquid electrolytes for rechargeable Li metal batteries. *Adv. Funct. Mater.* 30, 191077.
26. Yang, H.C., Li, J., Sun, Z.H., Fang, R.P., Wang, D.W., He, K., Cheng, H.M., and Li, F. (2020). Reliable liquid electrolytes for lithium metal batteries. *Energy Storage Mater.* 30, 113–129.
27. Zhai, P., Liu, L., Gu, X., Wang, T., and Gong, Y. (2020). Interface engineering for lithium metal anodes in liquid electrolyte. *Adv. Energy Mater.* 10, 2001257.
28. Tan, Y.H., Lu, G.X., Zheng, J.H., Zhou, F., Chen, M., Ma, T., Lu, L.L., Song, Y.H., Guan, Y., Wang, J., et al. (2021). Lithium fluoride in electrolyte for stable and Safe Lithium-Metal Batteries. *Adv. Mater.* 33, e2102134.
29. Manthiram, A., Yu, X., and Wang, S. (2017). Lithium battery chemistries enabled by solid-state electrolytes. *Nat. Rev. Mater.* 2, 16103.
30. Yang, X., Luo, J., and Sun, X. (2020). Towards high-performance solid-state Li-S batteries: from fundamental understanding to engineering design. *Chem. Soc. Rev.* 49, 2140–2195.
31. Zhang, X., Yang, Y., and Zhou, Z. (2020). Towards practical lithium-metal anodes. *Chem. Soc. Rev.* 49, 3040–3071.
32. Wu, F., Maier, J., and Yu, Y. (2020). Guidelines and trends for next-generation rechargeable lithium and lithium-ion batteries. *Chem. Soc. Rev.* 49, 1569–1614.
33. Liu, C., Neale, Z.G., and Cao, G. (2016). Understanding electrochemical potentials of cathode materials in rechargeable batteries. *Mater. Today* 19, 109–123.
34. Miao, X.G., Wang, H.Y., Sun, R., Wang, C.X., Zhang, Z.W., Li, Z.Q., and Yin, L.W. (2020). Interface engineering of inorganic solid-state electrolytes for high-performance lithium metal batteries. *Energy Environ. Sci.* 13, 3780–3822.
35. Quararone, E., and Mustarelli, P. (2011). Electrolytes for solid-state lithium rechargeable batteries: Recent advances and perspectives. *Chem. Soc. Rev.* 40, 2525–2540.
36. Kato, Y., Hori, S., Saito, T., Suzuki, K., Hirayama, M., Mitsui, A., Yonemura, M., Iba, H., and Kanno, R. (2016). High-power all-solid-state batteries using sulfide superionic conductors. *Nat. Energy* 1, 16030.
37. Qian, J., Wang, S., Li, Y., Zhang, M., Wang, F., Zhao, Y., Sun, Q., Li, L., Wu, F., and Chen, R. (2020). Lithium induced nano-sized copper with exposed lithiophilic surfaces to achieve dense lithium deposition for lithium metal anode. *Adv. Funct. Mater.* 31, 2006950.
38. Xu, Z., Chu, X., Wang, Y., Zhang, H., and Yang, W. (2020). Three-dimensional polymer networks for solid-state electrochemical energy storage. *Chem. Eng. J.* 391, 123548.
39. Zhou, W., Wang, Z., Pu, Y., Li, Y., Xin, S., Li, X., Chen, J., and Goodenough, J.B. (2019). Double-layer polymer electrolyte for high-voltage all-solid-state rechargeable batteries. *Adv. Mater.* 31, e1805574.
40. Tu, Q., Barroso-Luque, L., Shi, T., and Ceder, G. (2020). Electrodeposition and mechanical stability at lithium-solid electrolyte interface during plating in solid-state batteries. *Cell Rep. Phys. Sci.* 1, 100106.
41. Xu, B., Li, X., Yang, C., Li, Y., Grundish, N.S., Chien, P.H., Dong, K., Manke, I., Fang, R., Wu, N., et al. (2021). Interfacial chemistry enables stable cycling of all-solid-state Li metal batteries at high current densities. *J. Am. Chem. Soc.* 143, 6542–6550.
42. Zeng, X.X., Yin, Y.X., Li, N.W., Du, W.C., Guo, Y.G., and Wan, L.J. (2016). Reshaping lithium plating/stripping behavior via bifunctional polymer electrolyte for room-temperature solid Li metal batteries. *J. Am. Chem. Soc.* 138, 15825–15828.
43. Xiao, Y., Wang, Y., Bo, S.-H., Kim, J.C., Miara, L.J., and Ceder, G. (2019). Understanding interface stability in solid-state batteries. *Nat. Rev. Mater.* 5, 105–126.
44. Pan, K., Zhang, L., Qian, W., Wu, X., Dong, K., Zhang, H., and Zhang, S. (2020). A Flexible Ceramic/polymer hybrid solid electrolyte for solid-state lithium metal batteries. *Adv. Mater.* 32, e2000399.
45. Xu, Z., Yang, T., Chu, X., Su, H., Wang, Z., Chen, N., Gu, B., Zhang, H., Deng, W., Zhang, H., and Yang, W. (2020). Strong Lewis acid-base and weak hydrogen bond synergistically enhancing ionic conductivity of poly(ethylene oxide)@SiO<sub>2</sub> electrolytes for a high rate capability Li-metal battery. *ACS Appl. Mater. Interfaces* 12, 10341–10349.
46. Hatzell, K.B., Chen, X.C., Cobb, C.L., Dasgupta, N.P., Dixit, M.B., Marbella, L.E., McDowell, M.T., Mukherjee, P.P., Verma, A., Viswanathan, V., et al. (2020). Challenges in lithium metal anodes for solid-state batteries. *ACS Energy Lett.* 5, 922–934.
47. Kamaya, N., Homma, K., Yamakawa, Y., Hirayama, M., Kanno, R., Yonemura, M., Kamiyama, T., Kato, Y., Hama, S., Kawamoto, K., and Mitsui, A. (2011). A lithium superionic conductor. *Nat. Mater.* 10, 682–686.
48. Seino, Y., Ota, T., Takada, K., Hayashi, A., and Tatsumisago, M. (2014). A sulphide lithium super ion conductor is superior to liquid ion conductors for use in rechargeable batteries. *Energy Environ. Sci.* 7, 627–631.
49. Baranowski, L.L., Heveran, C.M., Ferguson, V.L., and Stoldt, C.R. (2016). Multi-scale mechanical behavior of the Li<sub>3</sub>PS<sub>4</sub> solid-phase electrolyte. *ACS Appl. Mater. Interfaces* 8, 29573–29579.
50. Ni, J.E., Case, E.D., Sakamoto, J.S., Rangasamy, E., and Wolfenstein, J.B. (2012). Room temperature elastic moduli and Vickers hardness of hot-pressed LLZO cubic garnet. *J. Mater. Sci.* 47, 7978–7985.
51. Shi, K., Wan, Z., Yang, L., Zhang, Y., Huang, Y., Su, S., Xia, H., Jiang, K., Shen, L., Hu, Y., et al. (2020). In situ construction of an ultra-stable conductive composite interface for high-voltage all-solid-state lithium metal batteries. *Angew. Chem. Int. Ed. Engl.* 59, 11784–11788.
52. Zhang, Z., Zhang, L., Liu, Y., Wang, H., Yu, C., Zeng, H., Wang, L.M., and Xu, B. (2018). Interface-engineered Li<sub>7</sub>La<sub>3</sub>Zr<sub>2</sub>O<sub>12</sub>-based garnet solid electrolytes with suppressed Li-dendrite formation and enhanced electrochemical performance. *ChemSusChem* 11, 3774–3782.
53. Huo, H., Li, X., Sun, Y., Lin, X., Doyle-Davis, K., Liang, J., Gao, X., Li, R., Huang, H., Guo, X., and Sun, X. (2020). Li<sub>2</sub>CO<sub>3</sub> effects: New insights into polymer/garnet electrolytes for dendrite-free solid lithium batteries. *Nano Energy* 73, 104836.
54. Lian, P.J., Zhao, B.S., Zhang, L.Q., Xu, N., Wu, M.T., and Gao, X.P. (2019). Inorganic sulfide solid electrolytes for all-solid-state lithium secondary batteries. *J. Mater. Chem. A*, 7, 20540–20557.
55. Liu, Z., Fu, W., Payzant, E.A., Yu, X., Wu, Z., Dudney, N.J., Kiggans, J., Hong, K., Rondinone, A.J., and Liang, C. (2013). Anomalous high ionic conductivity of nanoporous β-Li<sub>3</sub>PS<sub>4</sub>. *J. Am. Chem. Soc.* 135, 975–978.
56. Ren, Y.Y., Shen, Y., Lin, Y.H., and Nan, C.W. (2015). Direct observation of lithium dendrites inside garnet-type lithium-ion solid electrolyte. *Electrochim. Commun.* 57, 27–30.
57. Suzuki, Y., Kami, K., Watanabe, K., Watanabe, A., Saito, N., Ohnishi, T., Takada, K., Sudo, R., and Imanishi, N. (2015). Transparent cubic garnet-type solid electrolyte of Al<sub>2</sub>O<sub>3</sub>-doped Li<sub>7</sub>La<sub>3</sub>Zr<sub>2</sub>O<sub>12</sub>. *Solid State Ion.* 278, 172–176.
58. Liu, F., Wang, L., Zhang, Z., Shi, P., Feng, Y., Yao, Y., Ye, S., Wang, H., Wu, X., and Yu, Y. (2020). A mixed lithium-ion conductive Li<sub>2</sub>S/Li<sub>2</sub>Se protection layer for stable lithium metal anode. *Adv. Funct. Mater.* 30, 2001607.
59. Tang, Y., Zhang, L., Chen, J., Sun, H., Yang, T., Liu, Q., Huang, Q., Zhu, T., and Huang, J. (2021). Electro-chemo-mechanics of lithium in solid state lithium metal batteries. *Energy Environ. Sci.* 14, 602–642.
60. Krauskopf, T., Richter, F.H., Zeier, W.G., and Janek, J. (2020). Physicochemical concepts of the lithium metal anode in solid-state batteries. *Chem. Rev.* 120, 7745–7794.
61. Shi, H., Qin, J., Huang, K., Lu, P., Zhang, C.J., Dong, Y., Ye, M., Liu, Z., and Wu, Z.S. (2020). A two-dimensional mesoporous polypyrrole-graphene oxide heterostructure as a dual-functional ion redistributor for dendrite-free lithium metal anodes. *Angew. Chem. Int. Ed. Engl.* 59, 12147–12153.
62. Ke, X., Wang, Y., Dai, L., and Yuan, C. (2020). Cell failures of all-solid-state lithium metal batteries with inorganic solid electrolytes: Lithium dendrites. *Energy Stor. Mater.* 33, 309–328.
63. Cao, D.X., Sun, X., Li, Q., Natan, A., Xiang, P.Y., and Zhu, H.L. (2020). Lithium dendrite in all-solid-state batteries: Growth mechanisms, suppression strategies, and characterizations. *Mater. 3*, 57–94.
64. Zhu, J., Li, X., Wu, C., Gao, J., Xu, H., Li, Y., Guo, X., Li, H., and Zhou, W. (2021). A multilayer ceramic electrolyte for all-solid-state Li batteries. *Angew. Chem. Int. Ed. Engl.* 60, 3781–3790.

65. Hongahally Basappa, R., Ito, T., Morimura, T., Bekarevich, R., Mitsuishi, K., and Yamada, H. (2017). Grain boundary modification to suppress lithium penetration through garnet-type solid electrolyte. *J. Power Sources* 363, 145–152.
66. Jin, Y., Liu, C., Zong, X., Li, D., Fu, M., Tan, S., Xiong, Y., and Wei, J. (2020). Interface engineering of  $\text{Li}_{1.3}\text{Al}_{0.3}\text{Ti}_{1.7}(\text{PO}_4)_3$  ceramic electrolyte via multifunctional interfacial layer for all-solid-state lithium batteries. *J. Power Sources* 460, 228125–228133.
67. Mo, F., Ruan, J., Sun, S., Lian, Z., Yang, S., Yue, X., Song, Y., Zhou, Y.N., Fang, F., Sun, G., et al. (2019). Inside or outside: Origin of lithium dendrite formation of all solid-state electrolytes. *Adv. Energy Mater.* 9, 1902123.
68. Liu, Y., Su, H., Li, M., Xiang, J., Wu, X., Zhong, Y., Wang, X., Xia, X., Gu, C., and Tu, J. (2021). In situ formation of a  $\text{Li}_3\text{N}$ -rich interface between lithium and argyrodite solid electrolyte enabled by nitrogen doping. *J. Mater. Chem. A* 9, 13531–13539.
69. Ping, W., Wang, C., Lin, Z., Hitz, E., Yang, C., Wang, H., and Hu, L. (2020). Reversible short-circuit behaviors in garnet-based solid-state batteries. *Adv. Energy Mater.* 10, 2000702.
70. Monroe, C., and Newman, J. (2005). The impact of elastic deformation on deposition kinetics at lithium/polymer interfaces. *J. Electrochem. Soc.* 152, A396–A404.
71. Sudo, R., Nakata, Y., Ishiguro, K., Matsui, M., Hirano, A., Takeda, Y., Yamamoto, O., and Imanishi, N. (2014). Interface behavior between garnet-type lithium-conducting solid electrolyte and lithium metal. *Solid State Ion.* 262, 151–154.
72. Nagao, M., Hayashi, A., Tatsumisago, M., Kanetsuku, T., Tsuda, T., and Kuwabata, S. (2013). In situ SEM study of a lithium deposition and dissolution mechanism in a bulk-type solid-state cell with a  $\text{Li}_2\text{S}-\text{P}_2\text{S}_5$  solid electrolyte. *Phys. Chem. Chem. Phys.* 15, 18600–18606.
73. Aguesse, F., Manalastas, W., Buannic, L., Lopez Del Amo, J.M., Singh, G., Llordés, A., and Kilner, J. (2017). Investigating the dendritic growth during full cell cycling of garnet electrolyte in direct contact with Li metal. *ACS Appl. Mater. Interfaces* 9, 3808–3816.
74. Zhang, L., Yang, T., Du, C., Liu, Q., Tang, Y., Zhao, J., Wang, B., Chen, T., Sun, Y., Jia, P., et al. (2020). Lithium whisker growth and stress generation in an in situ atomic force microscope-environmental transmission electron microscope set-up. *Nat. Nanotechnol.* 15, 94–98.
75. Tsai, C.L., Roddatis, V., Chandran, C.V., Ma, Q., Uhlenbruck, S., Bram, M., Heitjans, P., and Guillou, O. (2016).  $\text{Li}_2\text{La}_3\text{Zr}_2\text{O}_{12}$  interface modification for Li dendrite prevention. *ACS Appl. Mater. Interfaces* 8, 10617–10626.
76. Tian, Y.J., Ding, F., Zhong, H., Liu, C., He, Y.B., Liu, J.Q., Liu, X.J., and Xu, Q. (2018).  $\text{Li}_{0.75}\text{La}_3\text{Zr}_{1.75}\text{Ta}_{0.25}\text{O}_{12}$ @amorphous  $\text{Li}_3\text{OCl}$  composite electrolyte for solid state lithium-metal batteries. *Energy Storage Mater.* 14, 49–57.
77. Cheng, E.J., Sharifi, A., and Sakamoto, J. (2017). Intergranular Li metal propagation through polycrystalline  $\text{Li}_{6.25}\text{Al}_{0.25}\text{La}_3\text{Zr}_2\text{O}_{12}$  ceramic electrolyte. *Electrochim. Acta* 223, 85–91.
78. Tippens, J., Miers, J.C., Afshar, A., Lewis, J.A., Cortes, F.J.Q., Qiao, H.P., Marchese, T.S., Di Leo, C.V., Saldana, C., and McDowell, M.T. (2019). Visualizing chemomechanical degradation of a solid-state battery electrolyte. *ACS Energy Lett.* 4, 1475–1483.
79. Kim, J.-S., Kim, H., Badding, M., Song, Z., Kim, K., Kim, Y., Yun, D.-J., Lee, D., Chang, J., Kim, S., et al. (2020). Origin of intergranular Li metal propagation in garnet-based solid electrolyte by direct electronic structure analysis and performance improvement by bandgap engineering. *J. Mater. Chem. A Mater. Energy Sustain.* 8, 16892–16901.
80. Liu, X., Garcia-Mendez, R., Lupini, A.R., Cheng, Y., Hood, Z.D., Han, F., Sharifi, A., Idrobo, J.C., Dudney, N.J., Wang, C., et al. (2021). Local electronic structure variation resulting in Li ‘filament’ formation within solid electrolytes. *Nat. Mater.* 20, 1485–1490.
81. Wu, B., Wang, S., Lochala, J., Desrochers, D., Liu, B., Zhang, W., Yang, J., and Xiao, J. (2018). The role of the solid electrolyte interphase layer in preventing Li dendrite growth in solid-state batteries. *Energy Environ. Sci.* 11, 1803–1810.
82. Qi, Y., Ban, C.M., and Harris, S.J. (2020). A new general paradigm for understanding and preventing Li metal penetration through solid electrolytes. *Joule* 4, 2599–2608.
83. Khokhar, W.A., Zhao, N., Huang, W., Wang, H., Bi, Z., and Guo, X. (2020). Different behaviors of metal penetration in Na and Li solid electrolytes. *ACS Appl. Mater. Interfaces* 12, 53781–53787.
84. Tantratian, K., Yan, H., Ellwood, K., Harrison, E.T., and Chen, L. (2021). Unraveling the Li penetration mechanism in polycrystalline solid electrolytes. *Adv. Energy Mater.* 11, 2003417.
85. Porz, L., Swamy, T., Sheldon, B.W., Rettenwander, D., Frömling, T., Thaman, H.L., Berendts, S., Uecker, R., Carter, W.C., and Chiang, Y.-M. (2017). Mechanism of lithium metal penetration through inorganic solid electrolytes. *Adv. Energy Mater.* 7, 1701003.
86. Bucci, G., and Christensen, J. (2019). Modeling of lithium electrodeposition at the lithium/ceramic electrolyte interface: The role of interfacial resistance and surface defects. *J. Power Sources* 441, 227186–227194.
87. Yu, S., and Siegel, D.J. (2018). Grain boundary softening: A potential mechanism for lithium metal penetration through stiff solid electrolytes. *ACS Appl. Mater. Interfaces* 10, 38151–38158.
88. Kazyak, E., Garcia-Mendez, R., LePage, W.S., Sharifi, A., Davis, A.L., Sanchez, A.J., Chen, K.-H., Haslam, C., Sakamoto, J., and Dasgupta, N.P. (2020). Li penetration in ceramic solid electrolytes: Operando microscopy analysis of morphology, propagation, and reversibility. *Matter* 2, 1025–1048.
89. Han, F.D., Westover, A.S., Yue, J., Fan, X.L., Wang, F., Chi, M.F., Leonard, D.N., Dudney, N., Wang, H., and Wang, C.S. (2019). High electronic conductivity as the origin of lithium dendrite formation within solid electrolytes. *Nat. Energy* 4, 187–196.
90. Song, Y., Yang, L., Zhao, W., Wang, Z., Zhao, Y., Wang, Z., Zhao, Q., Liu, H., and Pan, F. (2019). Revealing the short-circuiting mechanism of garnet-based solid-state electrolyte. *Adv. Energy Mater.* 9, 1900671.
91. Maslyn, J.A., Loo, W.S., McEntush, K.D., Oh, H.J., Harry, K.J., Parkinson, D.Y., and Balsara, N.P. (2018). Growth of lithium dendrites and globules through a solid block copolymer electrolyte as a function of current density. *J. Phys. Chem. C* 122, 26797–26804.
92. Barai, P., Ngo, A.T., Narayanan, B., Higa, K., Curtiss, L.A., and Srinivasan, V. (2020). The role of local inhomogeneities on dendrite growth in LLZO-based solid electrolytes. *J. Electrochem. Soc.* 167, 100537.
93. Lu, Y., Zhao, C.Z., Yuan, H., Cheng, X.B., Huang, J.Q., and Zhang, Q. (2021). Critical current density in solid-state lithium metal batteries: Mechanism, influences, and strategies. *Adv. Funct. Mater.* 31, 2009925.
94. Liu, H., Cheng, X.-B., Huang, J.-Q., Yuan, H., Lu, Y., Yan, C., Zhu, G.-L., Xu, R., Zhao, C.-Z., Hou, L.-P., et al. (2020). Controlling dendrite growth in solid-state electrolytes. *ACS Energy Lett.* 5, 833–843.
95. Mickal, D., Sannier, L., Beaudoin, B., Trentin, M., and Tarascon, J.-M. (2002). Live scanning electron microscope observations of dendritic growth in lithium/polymer cells. *Electrochem. Solid-State Lett.* 5, A286–A289.
96. Westover, A.S., Dudney, N.J., Sacci, R.L., and Kalnaus, S. (2019). Deposition and confinement of Li metal along an artificial lipon-lipon interface. *ACS Energy Lett.* 4, 651–655.
97. Guo, W., Shen, F., Liu, J., Zhang, Q., Guo, H., Yin, Y., Gao, J., Sun, Z., Han, X., and Hu, Y. (2021). In-situ optical observation of Li growth in garnet-type solid state electrolyte. *Energy Storage Mater.* 41, 791–797.
98. Golozar, M., Hovington, P., Paoletta, A., Bessette, S., Lagacé, M., Bouchard, P., Demers, H., Gauvin, R., and Zaghib, K. (2018). In situ scanning electron microscopy detection of carbide nature of sendrites in Li-polymer batteries. *Nano Lett.* 18, 7583–7589.
99. Wang, C., Gong, Y., Dai, J., Zhang, L., Xie, H., Pastel, G., Liu, B., Wachsman, E., Wang, H., and Hu, L. (2017). In situ neutron depth profiling of Lithium metal-garnet interfaces for solid state batteries. *J. Am. Chem. Soc.* 139, 14257–14264.
100. Marbella, L.E., Zekoll, S., Kasemchainan, J., Emge, S.P., Bruce, P.G., and Grey, C.P. (2019).  $^7\text{Li}$  NMR chemical shift Imaging to detect microstructural growth of lithium in all-solid-state batteries. *Chem. Mater.* 31, 2762–2769.
101. Ning, Z., Jolly, D.S., Li, G., De Meyere, R., Pu, S.D., Chen, Y., Kasemchainan, J., Ihli, J., Gong, C., Liu, B., et al. (2021). Visualizing plating-induced cracking in lithium-anode solid-electrolyte cells. *Nat. Mater.* 20, 1121–1129.

102. Sun, M., Liu, T., Yuan, Y., Ling, M., Xu, N., Liu, Y., Yan, L., Li, H., Liu, C., Lu, Y., et al. (2021). Visualizing lithium dendrite formation within solid-state electrolytes. *ACS Energy Lett.* 6, 451–458.
103. Zheng, J., Tang, M., and Hu, Y.Y. (2016). Lithium ion pathway within  $\text{Li}_7\text{La}_3\text{Zr}_2\text{O}_{12}$ -polyethylene oxide composite electrolytes. *Angew. Chem. Int. Ed. Engl.* 55, 12538–12542.
104. Harry, K.J., Hallinan, D.T., Parkinson, D.Y., MacDowell, A.A., and Balsara, N.P. (2014). Detection of subsurface structures underneath dendrites formed on cycled lithium metal electrodes. *Nat. Mater.* 13, 69–73.
105. Shen, F., Dixit, M.B., Xiao, X., and Hatzell, K.B. (2018). Effect of pore connectivity on Li dendrite propagation within LLZO electrolytes observed with synchrotron x-ray tomography. *ACS Energy Lett.* 3, 1056–1061.
106. Hao, S., Daemi, S.R., Heenan, T.M.M., Du, W., Tan, C., Storm, M., Rau, C., Brett, D.J.L., and Shearing, P.R. (2021). Tracking lithium penetration in solid electrolyte in 3D by in-situ synchrotron x-ray computed tomography. *Nano Energy* 82, 105744.
107. Krauskopf, T., Dippel, R., Hartmann, H., Peppler, K., Mogwitz, B., Richter, F.H., Zeier, W.G., and Janek, J. (2019). Lithium-metal growth kinetics on LLZO garnet-type solid electrolytes. *Joule* 3, 2030–2049.
108. Lu, Z., Yang, Z., Li, C., Wang, K., Han, J., Tong, P., Li, G., Vishnugopli, B.S., Mukherjee, P.P., Yang, C., and Li, W. (2021). Modulating nanoinhomogeneity at electrode–solid electrolyte interfaces for dendrite-proof solid-state batteries and long-life memristors. *Adv. Energy Mater.* 11, 2003811.
109. Sina, S., Roland, S., Ivan, P., Juri, B., Simon, P.R., Shicheng, Y., Simon, W., Samare, R., Hans, K., Karsten, R., et al. (2021). Nano-scale complexions facilitate Li dendrite-free operation in LATP solid-state electrolyte. *Adv. Energy Mater.* 11, 2100707.
110. Liu, J., Yuan, H., Liu, H., Zhao, C.Z., Lu, Y., Cheng, X.B., Huang, J.Q., and Zhang, Q. (2021). Unlocking the failure mechanism of solid state lithium metal batteries. *Adv. Energy Mater.* 2100748. Published online June 1, 2021. 10.1002/aenm.202100748.
111. Li, G., and Monroe, C.W. (2019). Dendrite nucleation in lithium-conductive ceramics. *Phys. Chem. Chem. Phys.* 21, 20354–20359.
112. Raj, R., and Wolfenstine, J. (2017). Current limit diagrams for dendrite formation in solid-state electrolytes for Li-ion batteries. *J. Power Sources* 343, 119–126.
113. Barai, P., Higa, K., and Srinivasan, V. (2017). Lithium dendrite growth mechanisms in polymer electrolytes and prevention strategies. *Phys. Chem. Chem. Phys.* 19, 20493–20505.
114. Tian, H.-K., Liu, Z., Ji, Y., Chen, L.-Q., and Qi, Y. (2019). Interfacial electronic properties dictate Li dendrite growth in solid electrolytes. *Chem. Mater.* 31, 7351–7359.
115. Ji, X., Hou, S., Wang, P., He, X., Piao, N., Chen, J., Fan, X., and Wang, C. (2020). Solid-state electrolyte design for lithium dendrite suppression. *Adv. Mater.* 32, e2002741.
116. Ren, Y., Zhou, Y., and Cao, Y. (2020). Inhibit of lithium dendrite growth in solid composite electrolyte by phase-field modeling. *J. Phys. Chem. C* 124, 12195–12204.
117. Yuan, C., Gao, X., Jia, Y., Zhang, W., Wu, Q., and Xu, J. (2021). Coupled crack propagation and dendrite growth in solid electrolyte of all-solid-state battery. *Nano Energy* 86, 106057.
118. Yu, S., and Siegel, D.J. (2017). Grain boundary contributions to Li-ion Transport in the Solid Electrolyte  $\text{Li}_7\text{La}_3\text{Zr}_2\text{O}_{12}$  (LLZO). *Chem. Mater.* 29, 9639–9647.
119. Ahmad, Z., and Viswanathan, V. (2017). Stability of electrodeposition at solid–solid interfaces and implications for metal anodes. *Phys. Rev. Lett.* 119, 056003.
120. Huo, H., Liang, J., Zhao, N., Li, X., Lin, X., Zhao, Y., Adair, K., Li, R., Guo, X., and Sun, X. (2020). Dynamics of the garnet/Li interface for dendrite-free solid-state batteries. *ACS Energy Lett.* 5, 2156–2164.
121. Zhao, J., Tang, Y., Dai, Q., Du, C., Zhang, Y., Xue, D., Chen, T., Chen, J., Wang, B., Yao, J., et al. (2021). In situ observation of Li deposition-induced cracking in garnet solid electrolytes. *Energy Environ. Mater.* 2575, 1232–1251. Published online August 15, 2021. 10.1002/eem.212261.
122. Lewis, J.A., Cortes, F.J.Q., Boebinger, M.G., Tippens, J., Marchese, T.S., Kondekar, N., Liu, X., Chi, M., and McDowell, M.T. (2019). Interphase morphology between a solid-state electrolyte and lithium controls cell failure. *ACS Energy Lett.* 4, 591–599.
123. Swamy, T., Park, R., Sheldon, B.W., Rettenwander, D., Porz, L., Berends, S., Uecker, R., Carter, W.C., and Chiang, Y.M. (2018). Lithium metal penetration induced by electrodeposition through solid electrolytes: Example in single-crystal  $\text{Li}_6\text{La}_3\text{TaO}_{12}$  garnet. *J. Electrochem. Soc.* 165, A3648–A3655.
124. Tian, H.K., Xu, B., and Qi, Y. (2018). Computational study of lithium nucleation tendency in  $\text{Li}_7\text{La}_3\text{Zr}_2\text{O}_{12}$  (LLZO) and rational design of interlayer materials to prevent lithium dendrites. *J. Power Sources* 392, 79–86.
125. Wang, M.J., Choudhury, R., and Sakamoto, J. (2019). Characterizing the Li–solid-electrolyte interface dynamics as a function of stack pressure and current density. *Joule* 3, 2165–2178.
126. Yuan, C., Lu, W., and Xu, J. (2021). Unlocking the electrochemical-mechanical coupling behaviors of dendrite growth and crack propagation in all-solid-state batteries. *Adv. Energy Mater.* 11, 2101807.
127. Li, Y., Wang, Z., Li, C., Cao, Y., and Guo, X. (2014). Densification and ionic-conduction improvement of lithium garnet solid electrolytes by flowing oxygen sintering. *J. Power Sources* 248, 642–646.
128. Yamada, H., Ito, T., and Hongahally Basappa, R. (2016). Sintering mechanisms of high-performance garnet-type solid electrolyte densified by spark plasma sintering. *Electrochim. Acta* 222, 648–656.
129. Yi, E., Wang, W., Kieffer, J., and Laine, R.M. (2016). Flame made nanoparticles permit processing of dense, flexible,  $\text{Li}^+$  conducting ceramic electrolyte thin films of cubic- $\text{Li}_7\text{La}_3\text{Zr}_2\text{O}_{12}$  (c-LLZO). *J. Mater. Chem. A* 4, 12947–12954.
130. Kumar, P.J., Nishimura, K., Senna, M., Düvel, A., Heijmans, P., Kawaguchi, T., Sakamoto, N., Wakiya, N., and Suzuki, H. (2016). A novel low-temperature solid-state route for nanostructured cubic garnet  $\text{Li}_7\text{La}_3\text{Zr}_2\text{O}_{12}$  and its application to Li-ion battery. *RSC Advances* 6, 62656–62667.
131. Sharifi, A., Meyer, H.M., Nanda, J., Wolfenstine, J., and Sakamoto, J. (2016). Characterizing the Li– $\text{Li}_7\text{La}_3\text{Zr}_2\text{O}_{12}$  interface stability and kinetics as a function of temperature and current density. *J. Power Sources* 302, 135–139.
132. Rangasamy, E., Wolfenstine, J., and Sakamoto, J. (2012). The role of Al and Li concentration on the formation of cubic garnet solid electrolyte of nominal composition  $\text{Li}_7\text{La}_3\text{Zr}_2\text{O}_{12}$ . *Solid State Ion.* 206, 28–32.
133. Ruan, Y., Lu, Y., Huang, X., Su, J., Sun, C., Jin, J., and Wen, Z. (2019). Acid induced conversion towards a robust and lithophilic interface for Li– $\text{Li}_7\text{La}_3\text{Zr}_2\text{O}_{12}$  solid-state batteries. *J. Mater. Chem. A* 7, 14565–14574.
134. Tang, S., Chen, G., Ren, F., Wang, H., Yang, W., Zheng, C., Gong, Z., and Yang, Y. (2021). Modifying an ultrathin insulating layer to suppress lithium dendrite formation within garnet solid electrolytes. *J. Mater. Chem. A* 9, 3576–3583.
135. Fu, J.M., Yu, P.F., Zhang, N., Ren, G.X., Zheng, S., Huang, W.C., Long, X.H., Li, H., and Liu, X.S. (2019). In situ formation of a bifunctional interlayer enabled by a conversion reaction to initiatively prevent lithium dendrites in a garnet solid electrolyte. *Energy Environ. Sci.* 12, 1404–1412.
136. Parejja, A., Amin, R., Essehlí, R., Wood, D.L., and Belharouak, I. (2020). Electrochemical healing of dendrites in garnet-based solid electrolytes. *ACS Energy Lett.* 5, 3368–3373.
137. Patra, S., Krupa, B.R., V., Chakravarty, S., and Murugan, R. (2019). Microstructural engineering in lithium garnets by hot isostatic press to cordon lithium dendrite growth and negate interfacial resistance for all solid state battery applications. *Electrochim. Acta* 312, 320–328.
138. Cheng, L., Chen, W., Kunz, M., Persson, K., Tamura, N., Chen, G., and Doeff, M. (2015). Effect of surface microstructure on electrochemical performance of garnet solid electrolytes. *ACS Appl. Mater. Interfaces* 7, 2073–2081.
139. Zhou, W., Zhu, Y., Grundish, N., Sen, X., Wang, S., You, Y., Wu, N., Gao, J., Cui, Z., Li, Y., and Goodenough, J.B. (2018). Polymer lithium-garnet interphase for an all-solid-state rechargeable battery. *Nano Energy* 53, 926–931.
140. Feng, W., Dong, X., Li, P., Wang, Y., and Xia, Y. (2019). Interfacial modification of Li/Garnet

- electrolyte by a lithophilic and breathing interlayer. *J. Power Sources* 419, 91–98.
141. Zheng, C., Ruan, Y., Su, J., Song, Z., Xiu, T., Jin, J., Badding, M.E., and Wen, Z. (2021). Grain boundary modification in garnet electrolyte to suppress lithium dendrite growth. *Chem. Eng. J.* 411, 128508.
  142. Kataoka, K., Nagata, H., and Akimoto, J. (2018). Lithium-ion conducting oxide single crystal as solid electrolyte for advanced lithium battery application. *Sci. Rep.* 8, 9965.
  143. Yin, Y., Jiang, C.-S., Guthrey, H., Xiao, C., Seitzman, N., Ban, C., and Al-Jassim, M. (2020). Improved stability and cyclability of ceramic solid electrolyte by coating polymer. *J. Electrochem. Soc.* 167, 020519.
  144. Wang, C., Gong, Y., Liu, B., Fu, K., Yao, Y., Hitz, E., Li, Y., Dai, J., Xu, S., Luo, W., et al. (2017). Conformal, nanoscale ZnO surface modification of garnet-based solid-state electrolyte for lithium metal anodes. *Nano Lett.* 17, 565–571.
  145. Han, X., Gong, Y., Fu, K.K., He, X., Hitz, G.T., Dai, J., Pearse, A., Liu, B., Wang, H., Rubloff, G., et al. (2017). Negating interfacial impedance in garnet-based solid-state Li metal batteries. *Nat. Mater.* 16, 572–579.
  146. Xu, R.C., Han, F.D., Ji, X., Fan, X.L., Tu, J.P., and Wang, C.S. (2018). Interface engineering of sulfide electrolytes for all-solid-state lithium batteries. *Nano Energy* 53, 958–966.
  147. Pervez, S.A., Ganjeh-Anzabi, P., Farooq, U., Trifkovic, M., Roberts, E.P.L., and Thangadurai, V. (2019). Fabrication of a dendrite-free all solid-state Li metal battery via polymer composite/garnet/polymer composite layered electrolyte. *Adv. Mater. Interfaces* 6, 1900186.
  148. Ye, L., and Li, X. (2021). A dynamic stability design strategy for lithium metal solid state batteries. *Nature* 593, 218–222.
  149. Zhou, W., Wang, S., Li, Y., Xin, S., Manthiram, A., and Goodenough, J.B. (2016). Plating a dendrite-free Lithium anode with a polymer/ceramic/polymer sandwich electrolyte. *J. Am. Chem. Soc.* 138, 9385–9388.
  150. Huo, H., Chen, Y., Luo, J., Yang, X., Guo, X., and Sun, X. (2019). Rational design of hierarchical “ceramic-in-polymer” and “polymer-in-ceramic” electrolytes for dendrite-free solid-state batteries. *Adv. Energy Mater.* 9, 1804004.
  151. Flatscher, F., Philipp, M., Ganschow, S., Wilkening, H.M.R., and Rettenwander, D. (2020). The natural critical current density limit for  $\text{Li}_7\text{La}_3\text{Zr}_2\text{O}_{12}$  garnets. *J. Mater. Chem. A* 8, 15782–15788.
  152. Fang, R., Xu, B., Grundish, N.S., Xia, Y., Li, Y., Lu, C., Liu, Y., Wu, N., and Goodenough, J.B. (2021).  $\text{Li}_2\text{S}_6$ -integrated PEO-based polymer electrolytes for all-solid-state Lithium-metal batteries. *Angew. Chem. Int. Ed. Engl.* 60, 17701–17706.
  153. Han, F., Yue, J., Zhu, X., and Wang, C. (2018). Suppressing Li dendrite formation in  $\text{Li}_2\text{S}-\text{P}_2\text{S}_5$  solid electrolyte by LiI incorporation. *Adv. Energy Mater.* 8, 1703644.
  154. Patra, S., Narayanasamy, J., Chakravarty, S., and Murugan, R. (2020). Higher critical current density in lithium garnets at room temperature by incorporation of an  $\text{Li}_4\text{SiO}_4$ -related glassy phase and hot isostatic pressing. *ACS Appl. Energy Mater.* 3, 2737–2743.
  155. Hosokawa, H., Takeda, A., Inada, R., and Sakurai, Y. (2020). Tolerance for Li dendrite penetration in Ta-doped  $\text{Li}_7\text{La}_3\text{Zr}_2\text{O}_{12}$  solid electrolytes sintered with  $\text{Li}_{2.3}\text{C}_{0.7}\text{B}_{0.3}\text{O}_3$  additive. *Mater. Lett.* 279, 128481–128485.
  156. Garcia-Mendez, R., Mizuno, F., Zhang, R., Arthur, T.S., and Sakamoto, J. (2017). Effect of processing conditions of  $75\text{Li}_2\text{S}-25\text{P}_2\text{S}_5$  solid electrolyte on its DC electrochemical behavior. *Electrochim. Acta* 237, 144–151.
  157. Pesci, F.M., Brugge, R.H., Hekselman, A.K.O., Cavallaro, A., Chater, R.J., and Aguadero, A. (2018). Elucidating the role of dopants in the critical current density for dendrite formation in garnet electrolytes. *J. Mater. Chem. A* 6, 19817–19827.
  158. Lu, G., Dong, Z., Liu, W., Jiang, X., Yang, Z., Liu, Q., Yang, X., Wu, D., Li, Z., Zhao, Q., et al. (2021). Universal lithophilic interfacial layers towards dendrite-free lithium anodes for solid-state lithium-metal batteries. *Sci. Bull. (Beijing)* 66, 1746–1753.
  159. Huo, H.Y., Chen, Y., Li, R.Y., Zhao, N., Luo, J., da Silva, J.G.P., Mucke, R., Kaghazchi, P., Guo, X.X., and Sun, X.L. (2020). Design of a mixed conductive garnet/Li interface for dendrite-free solid lithium metal batteries. *Energy Environ. Sci.* 13, 127–134.
  160. Shi, Y., Wan, J., Liu, G.X., Zuo, T.T., Song, Y.X., Liu, B., Guo, Y.G., Wen, R., and Wan, L.J. (2020). Interfacial evolution of Lithium dendrites and their solid electrolyte interphase shells of quasi-solid-state lithium-metal batteries. *Angew. Chem. Int. Ed. Engl.* 59, 18120–18125.
  161. Zhang, X., Wang, S., Xue, C., Xin, C., Lin, Y., Shen, Y., Li, L., and Nan, C.W. (2019). Self-suppression of lithium dendrite in all-solid-state lithium metal batteries with poly(vinylidene difluoride)-based solid electrolytes. *Adv. Mater.* 31, e1806082.
  162. Lukatskaya, M.R., Dunn, B., and Gogotsi, Y. (2016). Multidimensional materials and device architectures for future hybrid energy storage. *Nat. Commun.* 7, 12647.
  163. Taylor, N.J., Stangeland-Molo, S., Haslam, C.G., Sharafi, A., Thompson, T., Wang, M., Garcia-Mendez, R., and Sakamoto, J. (2018). Demonstration of high current densities and extended cycling in the garnet  $\text{Li}_7\text{La}_3\text{Zr}_2\text{O}_{12}$  solid electrolyte. *J. Power Sources* 396, 314–318.
  164. Um, J.H., and Yu, S.H. (2020). Unraveling the mechanisms of lithium metal plating/stripping via *in situ/operando* analytical techniques. *Adv. Energy Mater.* 11, 2003004.
  165. Liu, X., Li, X., Li, H., and Wu, H.B. (2018). Recent progress of hybrid solid-state electrolytes for lithium batteries. *Chemistry* 24, 18293–18306.